ABSTRACT

STUDY AND DEVELOPMENT OF ULTRASOUND MONITORING OF SKELETAL DEFECTS

by
Kavil Patel

Fatigue fractures are fine disruptions of normal bone architecture whose identification is often unreliable or difficult using x-rays (Robinson, Wilson et al.; Kundel 2004; Swischuk and Hernandez 2004). A fatigue fracture results from the application of abnormal loads to a bone with normal elastic resistance and is associated with new or different activity, and strenuous or repeated activity. The feasibility of using ultrasound to detect and monitor fatigue fractures and other structural damage in bone was established in this study.

The use of Low Transient Pulse (LTP) technology to drive the ultrasound transducers proved to enhance detection resolution and quality of the ultrasound signal in comparison to the use of conventional rectangular drive pulse. Sawbone plates mimicking the properties of cortical bone and cancellous bone were used to create limb phantoms with different cut depths.

A series of tests were conducted on these phantoms using Low Transient Pulse technology to demonstrate which design setup and signal parameters would maximize the sensitivity and specificity of the detection of fractures. Final experiments were carried out on sheep tibia simulating different fracture depths to prove the ability of ultrasound to detect fractures in an actual physiological environment.

STUDY AND DEVELOPMENT OF ULTRASOUND MONITORING OF SKELETAL DEFECTS

by
Kavil Patel

A Thesis
Submitted to the Faculty of
New Jersey Institute of Technology
in Partial Fulfillment of the Requirements for the Degree of
Master of Science in Biomedical Engineering

Department of Biomedical Engineering

January 2009

Blank Page

APPROVAL PAGE

STUDY AND DEVELOPMENT OF ULTRASOUND MONITORING OF SKELETAL DEFECTS

Kavil Patel

12/12/08

Dr. William C. Van Buskirk, Thesis Co-Advisor — Date
Distinguished Professor of Biomedical Engineering, NJIT

12/12/08

Dr. Timothy N. Chang, Thesis Co-Advisor — Date
Professor of Electrical and Computer Engineering, NJIT

12/12/08

Dr. Max Roman, Thesis Committee Member — Date
Research Professor of Biomedical Engineering, NJIT

BIOGRAPHICAL SKETCH

Author: Kavil Patel

Degree: Master of Science

Date: January 2009

Undergraduate and Graduate Education:

- Master of Science in Biomedical Engineering,
  New Jersey Institute of Technology, Newark, NJ, 2009

- Bachelor of Science in Bioengineering,
  Minor in Engineering Mechanics
  The Pennsylvania State University, University Park, PA, 2007

Major: Biomedical Engineering

"A discovery is said to be an accident meeting a prepared mind."

-by Albert Szent-Gyorgyi

I would like to dedicate this thesis to my beloved family for providing me with opportunity to receive the best education possible. I also appreciate my family's and friends' encouragement and understanding in whatever path I chose.

ACKNOWLEDGEMENT

I would like to express my deepest appreciation to Dr. Timothy N. Chang for his assistance and guidance not only as an advisor but as a great mentor. Thanks to Dr. Van Buskirk for providing me with the wonderful opportunity of working on this project. Special thanks to Dr. Max Roman for actively participating in my committee. The exposure to research and learning how to obtain and present information are invaluable tools that I will utilize throughout my career. I also owe a great deal of thanks to Biao Cheng for helping me understand and solve problems faced during the course of this study. I would also like to thank Celia Keim for her help and comments on the manuscript.

TABLE OF CONTENTS

Chapter	Page
1 INTRODUCTION	1
1.1 Objective	1
1.2 Background	1
1.2.1 Fatigue Fractures	1
1.2.2 Fatigue Fracture Diagnosis Quality	2
1.2.3 Quality vs. Quantitative Measurement	4
1.2.4 Quantative Ultrasound	4
2 EXPERIMENTAL SYSTEM AND TECHNOLOGY	6
2.1 Experimental Setup	6
2.2 Field Programmable Gate Array	7
2.3 Low Transient Pulse Technology	7
2.4 Transducer and Amplifier	10
2.5 Limb Phantom	12
2.5.1 Short Fiber Filled Epoxy Sheets (Sawbone Plate)	13
2.5.2 Cellular Rigid Polyurethane Foam	13
2.5.3 Sheep Tibia	14
2.5.4 Artificial Soft Tissue (Blue Phantom)	15
2.6 Transducer Mounting	15
2.7 Transducer Placement	17
2.8 Simulating Fractures	19

TABLE OF CONTENTS
(Continued)

Chapter **Page**

2.9 Signal Processing.. 22

3 PRELIMINARY STUDIES.. 25

3.1 Drive Signal Configuration.. 25

3.2 Transducer Characteristics.. 29

3.3 Mapping of Echoes.. 31

3.3.1 Simulation Analysis.. 32

3.3.2 Mapping Origin of Echoes.. 33

4 RESULTS AND ANALYSIS.. 37

4.1 Fracture Detection by Regular Rectangular Pulse and LTP 37

4.1 Sheep Tibia.. 39

4.2 Sawbone Plate.. 47

5 CONCLUSION.. 49

APPENDIX.. 51

REFERENCES.. 56

LIST OF TABLES

Table		Page
2.1	Parameters of the two-pulse LTP drive signal from n=3 and m=2..........	10
2.2	Biomechanical properties of Short Fiber Filled Epoxy Sheets	13
2.3	Biomechanical properties of Cellular Rigid Polyurethane Foam...........	14
4.1	Average values of flight time of the signal at R1 and R2 for both setups...	40
4.2	Average values of maximum amplitude of the signal at R1 and R2.........	42
4.3	Phase shift values for acoustic signal captured by R2 in setup 1............	45
4.4	Phase shift values for acoustic signal captured by R2 in setup 2............	45
4.5a	Correlation coefficient values of acoustic signal captured in setup 1........	46
4.5b	Correlation coefficient values of acoustic signal captured in setup 2........	46
4.6	Peak frequency captured at R1 and R2 for each cut depth..................	48

LIST OF FIGURES

Figure		Page
1.1	Fatigue fracture of distal second metatarsal..................................	3
1.2	Triple phase nuclear bone scan indicating the presence of the fatigue fracture of the distal second metatarsal..	3
2.1	Experimental Setup..	6
2.2	The Low Transient Pulse design scheme.....................................	8
2.3	Drive signals (top), acoustic signals (middle), and receiver outputs (bottom)..	10
2.4a	Frequency spectrum plot for transducer # 1 and transducer # 2.............	11
2.4b	Frequency spectrum plot for transducer #1 and transducer # 3..............	11
2.4c	Frequency Spectrum plot for transducer # 2 and transducer # .3............	12
2.5	Short Fiber Filled Epoxy Sheets (Sawbone Plates)..........................	13
2.6	Cellular Rigid Polyurethane Foam	14
2.7a	Designed fixture to hold the plate and transducer.............................	16
2.7b	Close-up of the fixture showing key components............................	16
2.8	First transducer placement setup configuration (setup 1)....................	18
2.9	Second transducer placement setup configuration (setup 2).................	19
2.10	Sawbone plate with a cut between receiver 1 (R1) and receiver 2 (R2).....	21
2.11a	Isometric view of sheep tibia..	22
2.11b	Cross section view of sheep tibia. Each line defines a fracture depth. Thin layer of glue is applied below the line to obtain desire fracture depth......	22
2.12	Acoustic signal showing parameters of interest................................	23
3.1	Low Transient Pulse generated with pulse period of 7.04 μs using the new FPGA system..	26

LIST OF FIGURES
(Continued)

Figure		Page
3.2a	Output captures using regular rectangular pulse as the drive signal......	27
3.2b	Output captured using Type 0 LTP (one pulse method) as the drive Signal........	27
3.2c	Output captured using Type 1 LTP (Two pulse method) as the drive Signal........	27
3.3a	Coefficient of Variance of LTP and RMP in the amplitude at R1...........	28
3.3b	Coefficient of Variance of LTP and RMP in the amplitude at R2...........	28
3.3c	Coefficient of Variance of LTP and RMP in the flight time at R1..........	28
3.3d	Coefficient of Variance of LTP and RMP in the flight time at R2..........	28
3.4a	Transducer #1 at position 1........	29
3.4b	Transducer #3 at position 1........	29
3.4c	Transducer #1 at position 2........	29
3.4d	Transducer #3 at position 2........	29
3.5a	Experimental setup showing two active transmitters and one receiver.....	30
3.5b	Experimental setup showing one active transmitters and one receiver.....	30
3.5c	Experimental setup showing one active transmitters and one receiver.....	30
3.6a	Output captured (Red) using only Transmitter 1 and output captured Blue) using only Transmitter 2........	31
3.6b	Experimental data (Red) captured when both transducers were running compared to sum of the two outputs (Blue) captured when transducer were used individually........	31
3.7	Block diagram of program constructed in simulink to generate waveform which matches experimental data........	32
3.8	Comparing experimental (red) waveform to waveform generated in simulink (blue)........	33

LIST OF FIGURES
(Continued)

Figure		Page
3.9	Compares the outputs captured in different arrangement which extend the boundary of the sawbone plate each time..................................	34
3.10a	Output signal captured on two sawbone plates stacked on top of each other without ultrasound gel in between.	35
310b	Output signal captured on two sawbone plates stacked on top of each other with layer of ultrasound gel between the two plates..................	35
4.1	Experimental setup for comparison of the LTP method and regular rectangular drive signal on the fracture detection.............................	37
4.2a	Signal received at R1 using regular rectangular pulse drive.................	38
4.2b	Signal received at R1 using LTP drive..	38
4.2c	Comparison of the received signals at R1..................................	38
4.3a	Signal received at R2 using regular rectangular pulse drive.................	38
4.3b	Signal received at R2 using LTP drive..	38
4.3c	Comparison of the received signals at R2..................................	38
4.4a	Setup 1 configuration...	39
4.4b	Setup 2 configuration...	39
4.5a	Flight time of acoustic signal captured by R1 in setup 1 vs. fracture depth	40
4.5b	Flight time of acoustic signal captured by R2 in setup 1 vs. fracture depth	40
4.5c	Flight time of acoustic signal captured by R1 in setup 2 vs. fracture depth	41
4.5d	Flight time of acoustic signal captures by R2 in setup 2 vs. fracture depth	41
4.6a	Maximum amplitude of acoustic signal captures by R1 in setup 1 vs. fracture depth...	43
4.6b	Maximum amplitude of acoustic signal captures by R2 in setup 1 vs. fracture depth...	43
4.6c	Maximum amplitude of acoustic signal captures by R1 in setup 2 vs. fracture depth...	43

LIST OF FIGURES
(Continued)

Figure		Page
4.6d	Maximum amplitude of acoustic signal captures by R2 in setup 2 vs. fracture depth..	43
4.6e	Ratiometric (R2/R1) representation of maximum amplitude of setup 1 vs. fracture depth...	44
4.6f	Ratiometric (R2/R1) representation of maximum amplitude of setup 2 vs. fracture depth..	44
4.7	Setup configuration...	47
4.8	Plot showing the behavior of the peak frequency of acoustic signal recorded at R1 and R2 with respect to different cut depths.................	48

CHAPTER 1

INTRODUCTION

1.1 Objective

The main purpose of this study was to demonstrate the feasibility of developing and utilizing an ultrasound based medical device for the detection and quantitative measurement of fatigue fractures and other structural damages to the bone. Some of the major tasks in this study involved implementing the Low Transient Pulse Technology to drive the ultrasound transducers and designing an experimental system that realized the proposed technology. The long term objective of this study is to develop a low cost portable hand-held diagnostic device that will supply, in real-time, quantitative measurements that will allow the physician to detect fracture and track the status of bone fractures from its initiation to healing.

1.2 Background

1.2.1 Fatigue Fractures

Fatigue fractures, also known as stress fractures, are one type of incomplete fracture in bone. Fatigue fractures are often seen as fine disruptions of normal bone architecture. These micro fractures are caused due to an activity such as running or jumping which exerts repetitive sub-threshold loading which over time exceeds bone's intrinsic ability to heal itself (Morris 1968). Fatigue fractures are commonly associated with athletes who run and jump on hard surfaces, such as distance runners, basketball players, and ballet dancers. Fatigue fractures are also known to occur in a deconditioned person who has just started a new exercise program, such as military recruits (Monteleone 1995; Maitra and Johnson 1997; Beck 1998). Fatigue fractures commonly occur in lower limbs as a result of the ground reaction forces that must be dissipated during running, walking, marching or jumping. Stress related fractures in the tibia account for approximately one-half of all stress fractures in children and adults, and fatigue fractures in metatarsals represent approximately 25% of stress fractures (Bennell and Brukner 1997; Brukner 2000). In adults approximately 10 % and in children about 20 % of fatigue fractures occur in distal end of fibula (Coady and Micheli 1997).

1.2.2 Fatigue Fracture Diagnosis Quality

Currently the most common methods of detecting fractures in bone are x-ray, MRI and CT. However, current technology used in detecting fatigue fractures is often unreliable, difficult and costly (Swischuk and Hernandez 2004)). Much of the misdiagnosis in fracture detection arises from the fractures that are simply too difficult to see with x-rays. A thorough review with suggestions for improvement demonstrates multiple fracture types that are easily missed in children (Swischuk and Hernandez 2004). Swischuk and Hernandez demonstrate that the fracture that may be unseen on a single x-ray is revealed when several x-rays from multiple vantage points and different angles are taken. The inability and uncertainty of plain radiograph films to indicate the presence of a fatigue fracture leaves the physician to resort to costlier methods, such as Magnetic Resonance Imaging (MRI) or Computed Tomography (CT). The presence of a fatigue fractures may not show up on plain radiograph film for up to 2 to 10 weeks after symptom onset, which increases the likelihood of a nonunion (Maitra and Johnson 1997; Callahan, Dillingham et al. 2011). Figure 1.1 below shows how plain radiograph fails to detect the presence of a fatigue fracture of the distal second metatarsals. When compared to an image obtained from triple base nuclear bone scan (Figure 1.2), a focal "hot spot" is shown on the image at the point of maximum tenderness.

Figure 1.1 Fatigue fracture of the distal second metatarsal. Initial Plain film Radiograph often unhelpful and does not indicate the presence of fatigue fracture (Sanderlin and Raspa 2003).

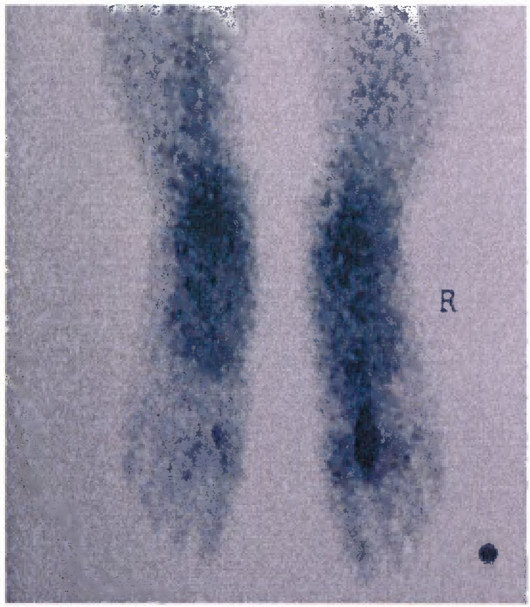

Figure 1.2 Triple phase nuclear bone scan indicating the presence of the fatigue fracture of the distal second metatarsal (Sanderlin and Raspa 2003).

The drawback of using a method which involves taking multiple x-rays at different vantage points to detect fatigue fracture is that the increased accuracy in diagnosis requires the patient to to absorb increased amounts of harmful radiation. Using bone scan, MRI or CT to carry out the diagnosis increases the cost of the treatment. This shows a need for a low cost diagnosis device which can detect fatigue fractures before it becomes a major fracture or results in a nonunion.

1.2.3 Qualitative vs. Quantitative Measurement

Current bone fracture monitoring methods such as x-rays, CTs and MRIs are all qualitative methods of identifying fractures as they require interpretation by highly trained and experienced physicians (Swischuk and Hernandez 2004). Although these tests can be performed repeatedly throughout the fracture life span, the cost of the treatment and the time spent by physicians and technicians interpreting the data makes this method prohibitive.

Along with the cost and time required by the physician for qualitative methods there is also a possibility of errors in the readings. These errors can be induced due to physicians' technique, perception, knowledge, judgment or communication (Fitzgerald 2001). Along with the errors there are also differences in diagnosis performed by two physicians. The qualitative nature of the tests is responsible for all the induced errors. These errors can be decreased by providing physicians with quantitative results. A device which provides quantitative results in monitoring bone fractures would decrease the dependability on experts to interpret the results and would also reduce the variance and increase accuracy in diagnosing a fracture.

1.2.4 Quantative Ultrasound

The use of Quantative Ultrasound System (QUS) has become more widespread in field of orthopedics due to its potential advantages over CT, MRI, and X-ray in terms of cost, size, safety, and detection resolution (Frost, Blake et al. 2002) . A number of studies have been conducted to investigate the use and reliability of QUS in detecting osteoporosis in patients. The underlying principle behind these ultrasound devices is to monitor the velocity of sound in bone, which is governed by the thickness of the cortical bone. As in these ultrasound devices only one parameter of acoustic signal is investigated the signal cannot be quantified properly to yield a proper diagnosis (Sarvazyan, Tatarinov et al. 2008). Also a major consideration of ultrasound imaging and QUS is the resolution. Traditionally, this resolution is achieved by increasing the frequency at the expense of reduced penetration and higher cost. Furthermore, sucessive signal packets tend to interfere with each other due to transducer transient which futher limit the detection resolution. The new Low Transient Pulse (LTP) technology, developed by NJIT and described in "System and Method for Pressure Wave Transmission and Measurement", teaches a method to compress acoustic pulses to pre-specified short durations. This technology can be a key enabling factor for better detection performance for an ultrasound diagnostic system when used in axial QUS. Axial QUS is a unique method which has a special placement among quantative ultrasound (Tatarinov, Sarvazyan et al. 2005). The axial QUS technique presents an advantage of unilateral positioning of the probe at available sites of long bones covered by a thin layer of soft tissue (Lowet and Van der Perre 1996; Camus, Talmant et al. 2000). This unilateral positioning of trandsucers allow capturing ultrasound surface waves progating along the bone axis and capturing mainly the compact bone.

CHAPTER 2

EXPERIMENTAL SYSTEM AND TECHNOLOGY

2.1 Experimental Setup

A Field Programmable Gate Array (FPGA) was programmed to synthesize and deliver a low transient pulse which was used as a drive signal for the ultrasonic transducer. As shown in Figure 2.1 the ultrasonic pulse is captured by sets of receivers which were placed on a specific specimen. A high bandwidth digital oscilloscope was used to capture the high frequency ultrasound signals. These captured signals are then analyzed and processed to obtain essential parameters which help in fracture detection. All the components of the experimental setup are explained in detail in the following section.

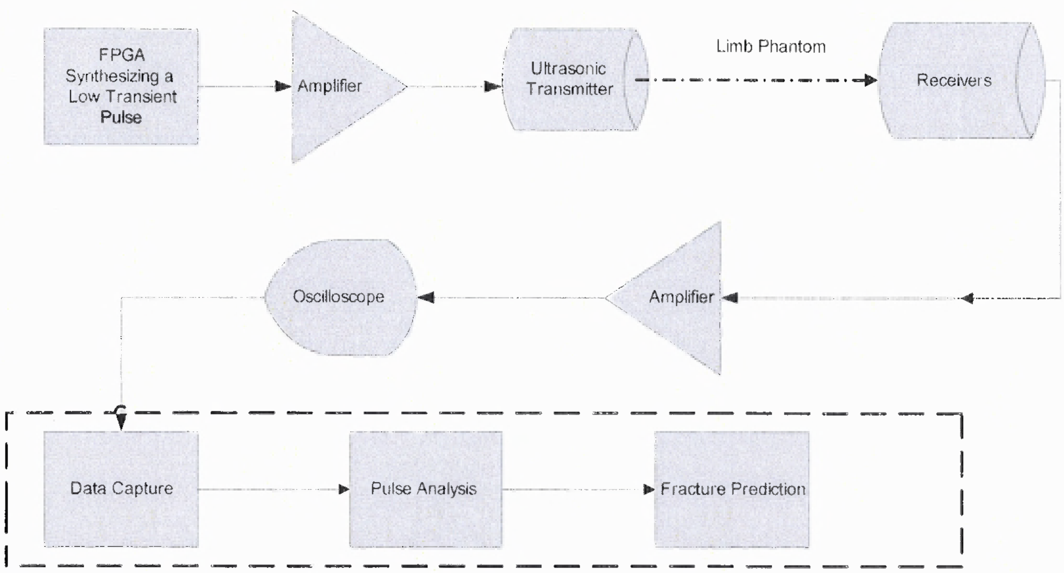

Figure 2.1 Experimental setup.

2.2 Field Programmable Gate Array

A field programmable gate array (FPGA) was used in this study to produce the Low Transient Pulse (LTP) drive signals for the transducers. A Dalanco Spry digital signal processing and data acquisition board model AVR-32 was used to generate the LTP. The board is a PCI bus, PC add –in card powered by Texas Instruments TMS320C32 Digital Signal Processor (DSP) and Xilinx Spartan Field Programmable Gate Array (FPGA). The configuration of the Spartan FPGA establishes the interaction of the D/A, and digital I/O with the local bus. The sampling rate of the D/A converter can be set by the timer in the DSP. The clock frequency of the FPGA was 62.5 MHz. For this study the combination of DSP and FPGA was used to synthesize a LTP drive signal. The combination of DSP and FPGA along with FPGA's high clock frequency generates a LTP drive signal with a high temporal resolution. The combination also provides flexibility in pulse design which makes configuration of LTP according to specimen characteristics an efficient process. The incrementing counter value at every clock frequency defines the pulse width of the LTP. Pulse width of the LTP drive signal was the only input required by the user. The pulse width of the drive signal was determined based on the frequency spectrum of the specimen. Running the program generates the pre-defined LTP.

2.3 Low Transient Pulse Technology

The low transient pulse (LTP) technology is an innovative technique to produce a short duration and low transient acoustic pulse by means of pre-shaping the excitation signal (Cheng and Chang 2007). It has been experimentally verified that the LTP method produces a better measurement resolution and simpler hardware implementation due to less phase interference and a less complex algorithm. No modulation circuits or regenerative loops are necessary to synthesize the drive signal.

The LTP method is based on the input shaping method which is a feedforward technique to suppress the command-induced vibratory transient of a system (Chang, Hou et al. 2003). Within the quantitative ultrasonography context, the LTP method improves detection resolution by minimizing aliasing of signals transmitted from soft and hard tissues. This improvement is achieved by convolving the input pulse width and impulse sequence to generate a necessary drive signal. Figure 2.2 below shows the pulse-impulse convolution scheme.

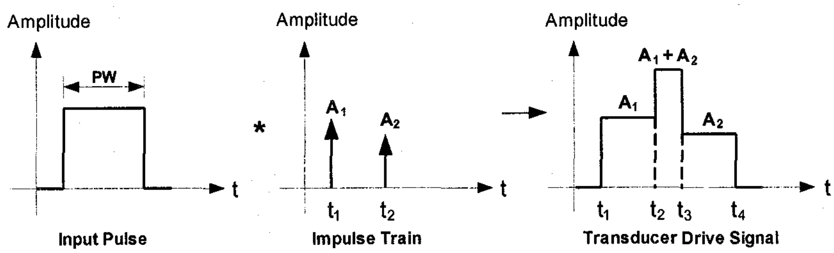

Figure 2.2 The Low Transient Pulse design scheme (Biao Cheng 2007).

The transducer drive signal so produced is then stored in a computer and later fed into the ultrasound transmitter. These impulse parameters are obtained by considering the transducer up to the first resonance using a second order system shown below.

$$G(s) = \frac{\alpha s}{s^2 + 2\zeta\omega_n s + \omega_n^2}$$

The design parameters of a two-impulse low transient pulse shaper can be obtained as follows,

$$\Delta T = \frac{n\pi}{\omega_n \sqrt{1-\zeta^2}} = \frac{n\pi}{\omega_d}, M_p^n = \left(e^{\frac{\zeta\pi}{\sqrt{1-\zeta^2}}} \right)^n, n = 1,3,5$$

where ΔT and M_p can be readily determined from the transducer calibration experiment. The variable n determines the oscillation cycles of the LTP signal. The transmitter-Receiver Optimized LTP drive signal will produce a low transient pulse on both the transmitter and receiver outputs. This is achieved by properly selecting the pulse width, so that the transients are cancelled at both transmitter and receiver side. The design parameters are given as following

$$A_1 = \frac{1}{1+M_p^n}, A_2 = \frac{M_p^n}{1+M_p^n},$$

$$t_1 = 0, t_2 = \Delta T, PW = \frac{4t_2}{3}, t_3 = \frac{4t_2}{3}, t_4 = \frac{7t_2}{3}$$

A Simulated transmitter drive signal, acoustic signal and receiver signal are shown in Figure 2.3. The Rectangular Modulation Pulse (RMP) drive and acoustic signal are depicted in Figure 2.3(a) while the LTP drive and acoustic signals are shown in Figure 2.3(b). For the RMP method, the excitation signal is a 400 Hz pulse train with 5 % duty cycle modulated by a 40 KHz sine wave. LTP pulse design parameters are shown in Table 2.1. When two pulse are compared it is evident that the conventional drive method suffers from longer transients which alias and impede quantitative analysis of the pulse signals. On the other hand the LTP drive signal produces clean distinct signals with lower transient (Cheng and Chang 2007).

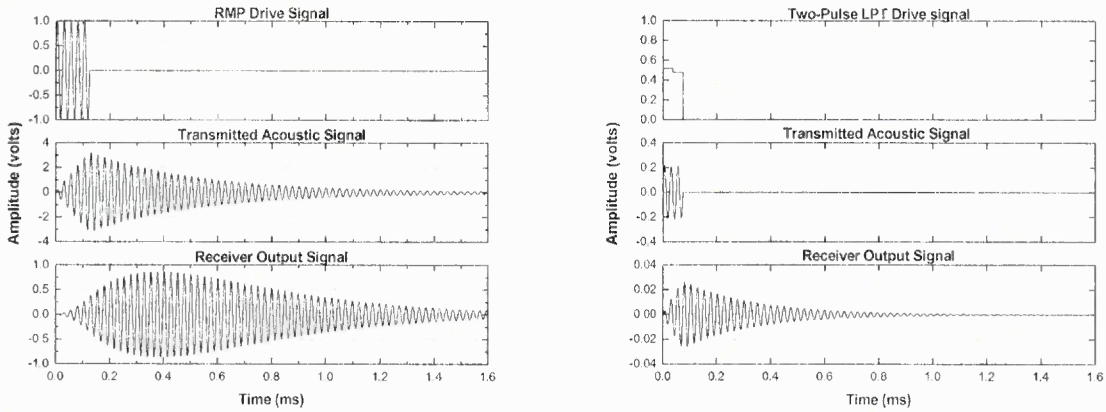

(a) RMP excitation (b) LTP excitation

Figure 2.3 Drive signals (top), acoustic signals (middle), and receiver outputs (bottom).

Table 2.1 Parameters of the two-pulse LTP drive signal for n = 3 and m = 2.

M_p^3	Δt (sec)	t_2 (sec)	A_1 (volts)	A_2 (volts)	PW (sec)
0.9144	3.7315×10^{-5}	3.7315×10^{-5}	0.5224	0.4776	3.7315×10^{-5}

2.4 Transducer and Amplifier

The transducers used in this study were general purpose R15α Frequency Acoustic Emission Sensor manufactured by Physical Acoustic Corporation. Three of these transducers were used throughout the entire course of the study. In order to keep track of which transducer was used at what position in a particular experiment they were tagged as transducer #1, transducer # 2 and transducer # 3. The active element of R15α acoustic transducer was piezoelectric ceramic. These R15α transducers had a resonant frequency of 150 KHz and had an operating frequency which ranged from 50-200 KHz. These transducers were used as transmitter as well as a receiver during the experiment. The transducer had a stainless steel outer casing and ceramic face plate which sits on the specimen. Each transducer weighs 34 grams and is 19 mm in diameter and 22.4 mm in height.

A simple input output calibration experiment was carried out to measure the experimental frequency response of the transducers. The transducers were arranged in direct coupling and a sine wave was used as a drive signal. The amplitude of the output signal at each frequency was recorded. The plot below in Figure 2.4 shows the frequency response of each transducer. From the plots below it was inferred that the resonant frequency of all three transducers was around 140 KHz and it was also confirmed that all transducers have matching acoustic characteristics.

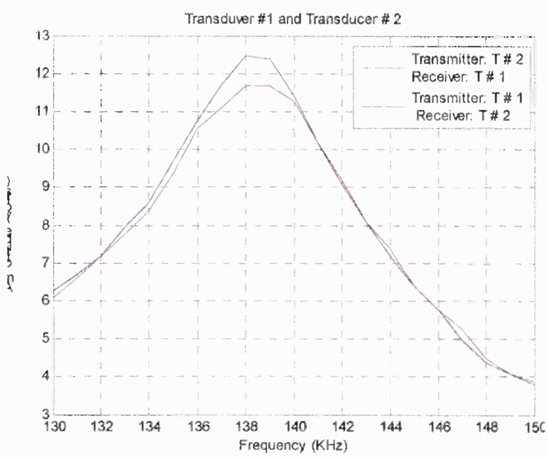

Figure 2.4a Frequency spectrum plot for transducer # 1 and transducer # 2.

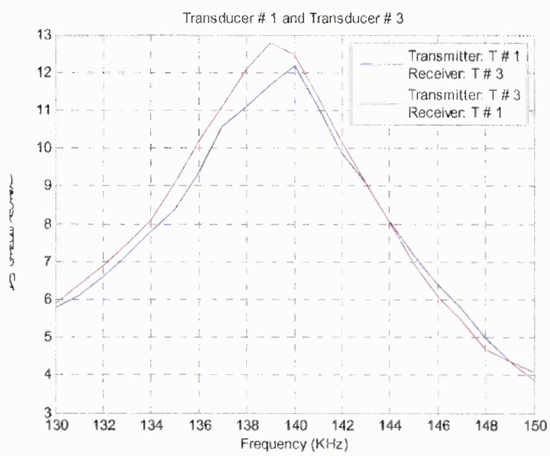

Figure 2.4b Frequency spectrum plot for transducer #1 and transducer # 3.

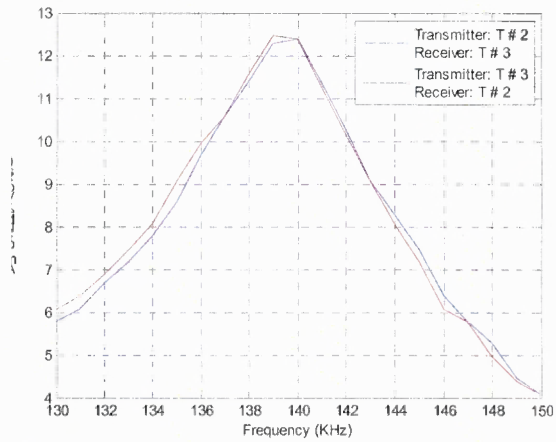

Figure 2.4c Frequency Spectrum plot for transducer # 2 and transducer # 3.

The amplifier used in this study was AE2A/AE5A Wide Bandwidth Acoustic Emission Amplifier System manufactured by Physical Acoustic Corporation. This AE2A/AE5A acoustic emission amplifier is a small and high performance acoustic emission system that amplifies and filters an incoming acoustic emission signal directly from an acoustic sensor. This model covers the entire traditional acoustic emission bandwidth up to 2 MHz. The acoustic emission amplifier was connected to the digital oscilloscope to view the output captured by the receiver.

2.5 Limb Phantom

Throughout the entire study materials were used which mimic the physical and acoustic properties of bone and soft tissue. Every material used in this study is listed and described below.

2.5.1 Short Fiber Filled Epoxy Sheets (Sawbone Plates)

The short fiber filled epoxy sheets manufactured by Sawbones, Inc are plates which are used as an alternative testing medium to human cortical bone (Figure 2.5). These sawbone plates are a mixture of short glass fibers and epoxy resin that has been pressure molded into sheets which mimic the properties of human cortical bone. The flat surface provides ease in carrying out basic testing and calibrating experiments. Table 2.2 below provides the biomechanical properties of the sawbone plate.

Table 2.2 Mechanical properties of Short Fiber Filled Epoxy Sheets (Sawbone Plates).

Density		Compressive		Tensile		
		Strength	Modulus	Strength	Modulus	Strain
Pcf	g/cc	MPa	GPa	MPa	Gpa	%
102	1.64	157	16.7	106	16.0	0.80

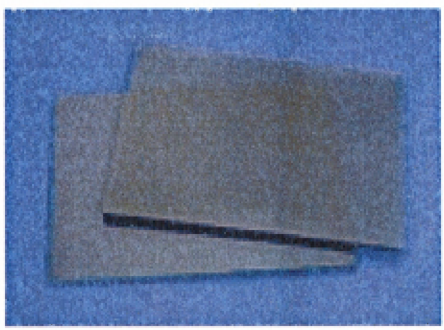

Figure 2.5 Short Fiber Filled Epoxy Sheets (Sawbone Plates).

2.5.2 Cellular Rigid Polyurethane Foam

The cellular rigid polyurethane foam testing blocks, manufactured by Sawbones, Inc were used as an alternative testing medium to human cancellous bone (Figure 2.6). Along with the biomechanical properties, the cellular rigid polyurethane foam blocks also mimic the same surface texture of cadaveric cancellous bone. Table 2.3 provides the biomechanical properties of the cellular rigid polyurethane foam.

Table 2.3 Biomechanical properties of Cellular Rigid Polyurethane Foam.

Density		Compressive		Cell Size
		Strength	Modulus	
pcf	g/cc	MPa	GPa	Mm
7.5	0.12	1.4	12.4	0.5-2.5

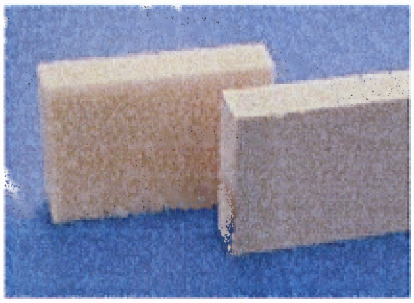

Figure 2.6 Cellular Rigid Polyurethane Foam.

2.5.3 Sheep Tibia

During the course of this study some experiments involved using the sheep tibia which allows mimicking a physiological environment. Four sheep tibia were obtained from the butcher shop. All the soft tissue on the bones was removed and cleaned. The bones were allowed to sit out in the open to dry.

2.5.4 Artificial Soft Tissue

The artificial soft tissue mimicking the acoustic characteristics of the actual soft tissue was used in some experiments to simulate an actual physiological environment. This artificial soft tissue is manufactured by a company called Blue Phantom. In a specific experiment the artificial soft tissue was sliced in thin layers and placed on top of sawbone or used to wrap sheep tibia. The artificial soft tissue was also used as a testing platform on which the sheep tibia was placed to create a barrier and ensure no reflections were created due to the experimental platform.

2.6 Transducer Mounting

Placement of the transducers was a very critical aspect of this study. The placement of transducers on sawbone plate and bone were required to be very precise due to the high sensitivity of ultrasound signal to the mounting site. The distance between the transmitter and the receiver and the amount of downward force applied on the transducers were the two factors which had to be controlled during an experiment. Any change in distance between the transducers can change the parameters of recorded signal. The downward force used to hold the transducers drives the impedance between the face plate of the transducer and the specimen surface; variability in this changes the amplitude of the recorded signal. In order to achieve a controlled environment a fixture was designed. Figure 2.7 shows the design fixture being used during an experiment. The fixture was mainly designed to carry out experiments with specimens with flat surfaces which mainly include the sawbone plates or a combination of sawbone plates and soft tissue. The fixture was designed such that the specimen was suspended above the testing platform by pointed screws which have a very small contact surface with the specimen. This feature allows eliminating the possibility of the testing platform interfering with the acoustic signal in the sawbone plate during the experiment. Three long screws with cushion pads were used to hold each transducer down by applying a constant downward force. Since this long screw runs along the threads in the top platform it assures that all the transducers are in a straight line providing a proper alignment and fixed distance between each transducer. The force applied to hold the transducers down to the sawbone plate can be regulated with the screws. The use to plastic material to manufacture the fixture allows it to be submerged in water for a long period of time without worrying about it rusting.

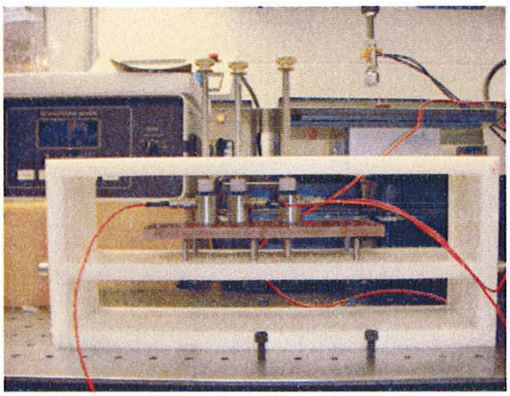

Figure 2.7a Designed fixture to hold the plate and transducer.

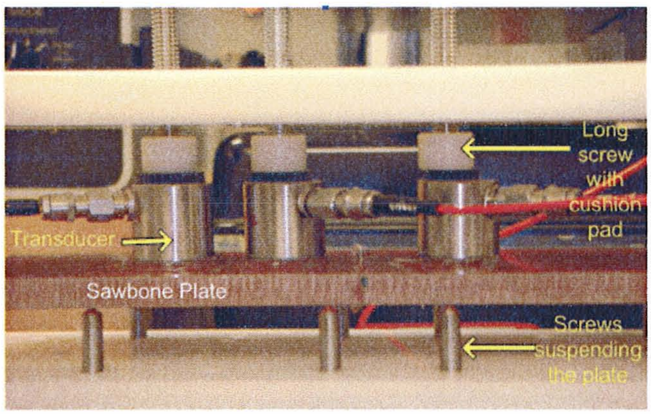

Figure 2.7b Close-up of the fixture showing key components.

Due to uneven surface of the bone, transducer placement on bone is difficult and the designed fixture could not be used. Simply having ultrasound gel between the transducer face plate and bone did not provide enough stability nor a good medium for transferring the acoustic energy. In experiments involving bone the transducers were mounted on the bone surface with synthetic bee wax glue. Bee wax glue provided stability and ensured that the transducers do not move from their mounting position providing a fixed distance between each transducer through the course of the experiment. This method also achieved a flush contact surface between the transducer faceplate and bone.

2.7 Transducer Placement

The ultrasound axial transmission method used in this study does not use ultrasonic reflection to characterize a material but passes the ultrasonic energy along a material and quantifies the effects the material has on the energy. This axial transmission testing procedure employs an ultrasonic technique known as axial quantitative ultrasound, which involves passing ultrasonic energy along the bone, instead of through the bone (Hubner, Schlicht et al. 2000; Knapp, Blake et al. 2004). Transducer placement in this technique is a significant factor. Transducer placements are the different combinations of distance between the transmitter, the receiver and their relation to the known fracture location. Every experiment setup on the limb phantom in this study involved three transducers, as shown in Figure 2.8. During the course of the study, two different setup configurations were used. The first setup configuration which was the most common setup used during the course of entire study is shown in Figure 2.8. In first setup (Setup 1) the first transducer is the transmitter (T1) and the received energy is recorded from two locations (R1 & R2) along the test sample. The reason for this setup is to produce a reference recording and test recording. In the first recording (R1), the reference is taken across a known healthy uninjured section of bone. The second recording (R2) is taken from across the suspected fracture location. The effect is that the reference recording is the signal affected by all individual local characteristics of the sample. The test recording taken across the fracture will be similarly affected by these same specific characteristics plus the characteristics of the fracture. Therefore, comparisons between the signals across the reference region and the injured region will only differ by the presence of the fracture and its status.

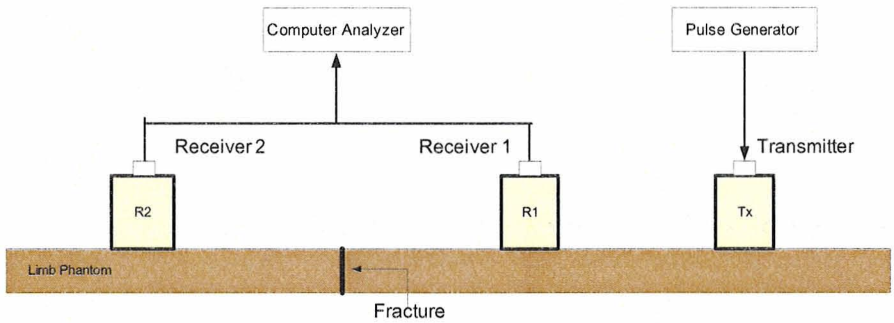

Figure 2.8 First transducer placement setup configuration (setup 1).

The second setup configuration (setup 2) shown in Figure 2.9 follows the same fundamental principles of first setup. As seen from Figure 2.9 the only thing that changes in this setup is the order in which the transmitter and receivers are placed. In second setup configuration the transmitter is placed between the two receivers. One of the receivers (R1) is placed on the unaffected side of the bone and the second receiver (R2) is placed across the fracture. This configuration, in conjunction with the first setup, gives added information regarding the fracture parameters.

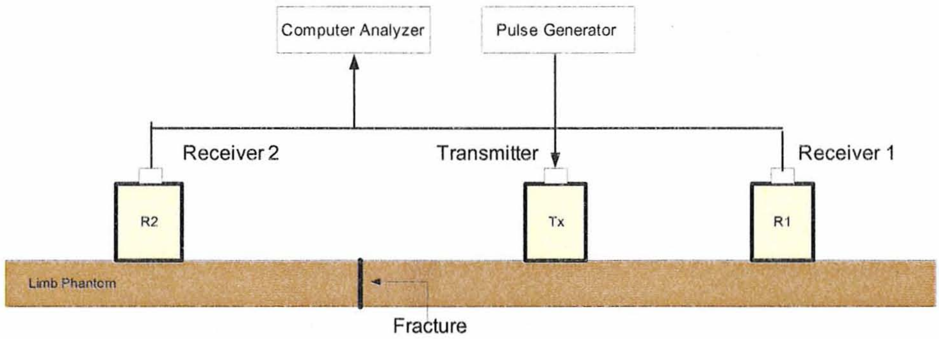

Figure 2.9 Second transducer placement setup configuration (setup 2).

The distance between transducers for both setup configurations is varied based on the experiment being performed. Varying the distance between the transducers allows investigating the effects of distance on the passage of energy through the limb phantom. Acoustic energy travels at speeds dependent on different material properties. The most significant factors are the density and elastic properties of the material. Therefore, energy packets traveling through bone and through soft tissue will be separate and arrive at the receivers at different time intervals. This separation in time intervals allows investigation of energy packets that have traveled through only soft tissue and energy packets that have only passed through bone.

2.8 Simulating Fractures

Three different techniques were used to simulate fractures depending on the testing scenario and material being used. For initial preliminary studies a simple method was used to simulate a bone fracture or a discontinuity. Three point bending load was applied to the sawbone plate and at the same time an electric saw was used to break the sawbone plate in half. When the broken edges of sawbone plate are re-joined with ultrasound gel in-between, the plate does not simulate any fracture, as the presence of ultrasound gel provides a good medium for transfer of acoustic energy. The depth and severity of the fracture could be regulated with the amount of gel applied between the two plates. The sawbone plate simulates a complete fracture when the broken edges of the sawbone plate are re-joined without any ultrasound gel in-between. These fracture characteristics are observed in the re-joined sawbone plate due to the presence of air pockets and low density medium between the connecting edges.

For experiments which required observing changes in signal characteristics as a discontinuity or cut of different depth was induced in the sawbone plate a different approach was used. To observe changes in signal characteristics only due to the introduction of a cut or change in the depth of the cut, it was important to keep the number of variables as low as possible. Due to high sensitivity of ultrasound to its environmental features, variability could be easily induced by a small change in placement or orientation of transducer, change in amount of gel in between the transducer face plate and specimen, and by difference in downward force applied on transducer by the fixture. In order to keep all of these variables constant the transducers were mounted on to the sawbone plate using bee wax. To observe the changes in recorded signal, a hack saw was used to introduce a cut in the plate. Series of cuts with different cut depth were created without disturbing the transducers and their placement. The setup provided enough place between the two receivers to place the hack saw between them and increase the cut depth. In this way, the recorded signal only addressed the changes occurring due to increase in cut depth. Figure 2.10 shows the sawbone plate with cut between R1 and

R2. Starting from no cut, different cuts having depth of 1.5 mm, 2.3 mm, 2.68 mm, and 2.83 mm were introduced in sawbone plate using the hack saw.

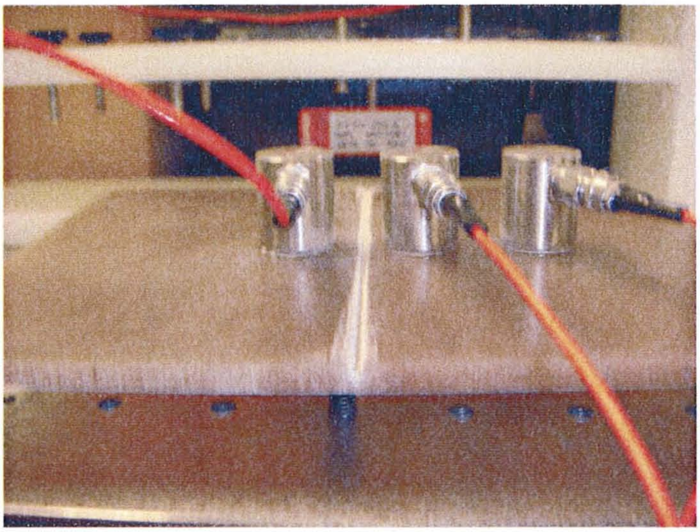

Figure 2.10 Sawbone plate with a cut between receiver 1 (R1) and receiver 2 (R2).

A new technique was designed to simulate a hairline fracture in sheep tibia which closely represents an actual fracture seen in physiological setting. This technique involved cutting the sheep tibia in two pieces at the center point of diaphysis using a thin electric band saw, polishing the cut edges and re-attaching them with different amount of super glue each time. At first it was important to study if the acoustic properties of super glue match the acoustic properties of the bone. The cut tibia was re-attached with application of super glue throughout the cross section of cortical and cancellous bone. It was made sure that only thin uniform film of super glue was applied along the cross section. A simple experiment was setup to compare acoustic signal captured by two receivers from an intact bone to the acoustic signal captured from bone re-attached with super glue throughout its cross section. The results confirmed that material density and damping coefficient of super glue match closely to the density of the bone as no major differences were observed in the signal characteristics between the two situations. The joined pieces of tibia were easily de-attached by applying shear force at the site of connection. Readings were then taken from the two mounted receivers in both setups after the bone was re-attached each time with different controlled levels of super glue. Cross section area where glue was applied is considered to be intact bone and area without glue in between simulates fracture. Different amount of glue yields fracture with different depth. Good care was taken during data collection to assure that the mounted transducers do not come off during the process of separating two pieces and re-attaching them. Fractures or discontinuity were simulated in sheep tibia with depth of 2.87 mm, 4.80 mm, 7.12 mm and 11.68mm.

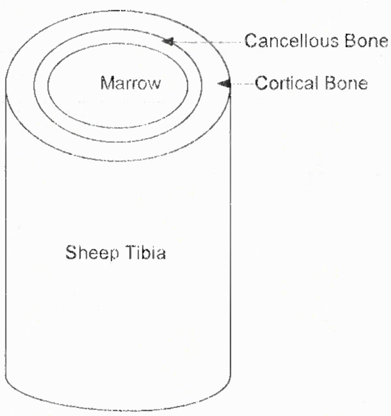

Figure 2.11a Isometric view of sheep tibia.

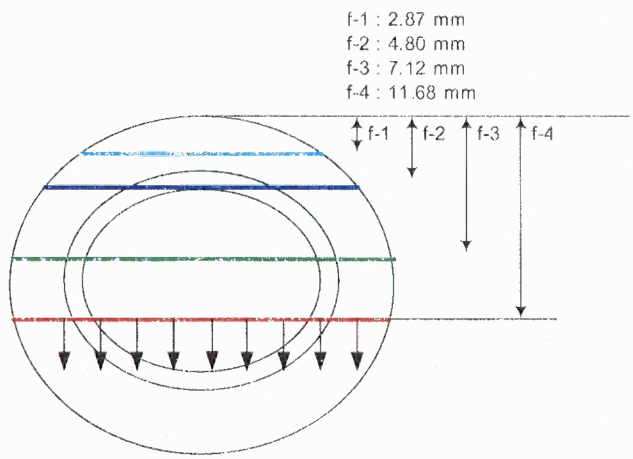

Figure 2.11b Cross section view of sheep tibia. Each line defines a fracture depth. Thin layer of glue is applied below the line to obtain desire fracture depth.

2.9 Signal Processing

The output signal captured by the receiver was recorded using the digital oscilloscope. The recorded signal was then analyzed to identify the parameters which are most sensitive and can quantify fracture in a bone. Figure 2.12 below shows the acoustic parameters of the signal which are of interest in this study. The flight time of the signal is

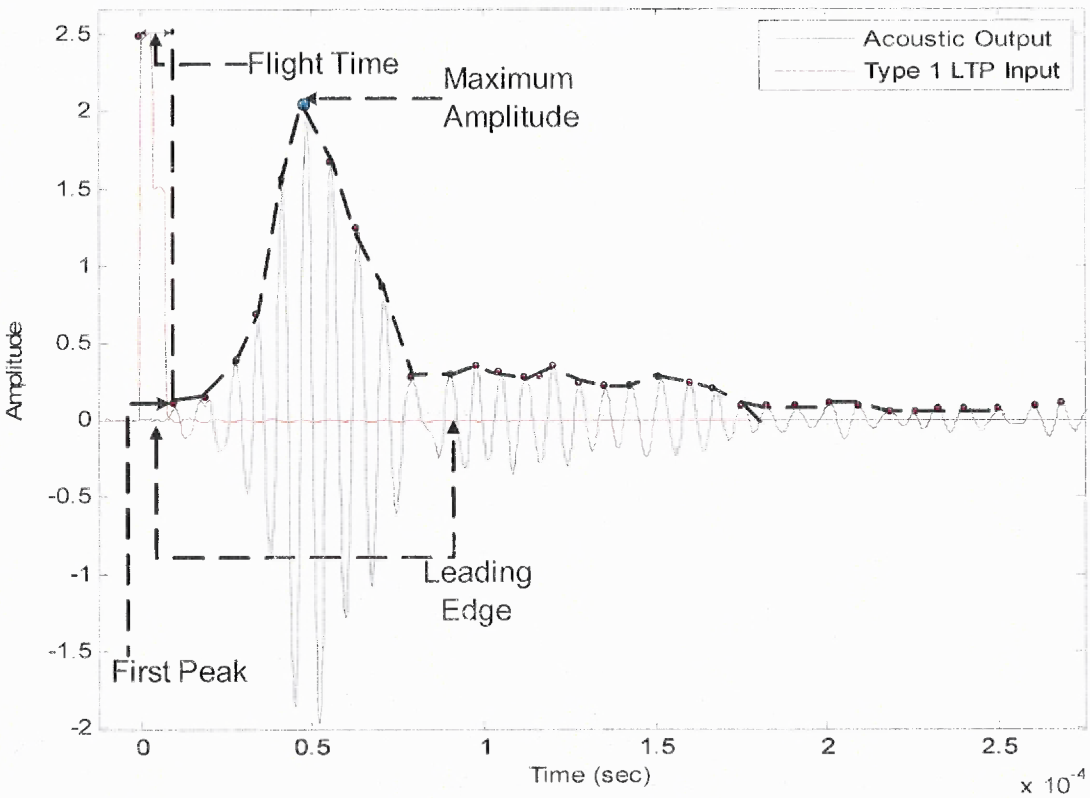

Figure 2.12 Acoustic signal showing parameters of interest.

one of the most important and widely used parameters used in ultrasound testing . Flight time is defined as time taken by the acoustic energy to travel along the bone from transmitter to the receiver. Additional experiments were carried to determine the right method for calculating flight time of the acoustic energy in this study. The traditional technique of using the highest peak of received signal as the endpoint of the flight time did not work in this study. Peaks present in reflection signals are sometimes higher in amplitude making the selection of the endpoint difficult. The first peak seen in the signal was selected as a reference point which determines the flight time. Also according to the theoretical calculation using the experimental velocity of the sound in bone and the known distance between the transducers, the calculated flight time of a particular signal lies close to the first peak seen in a signal captured from an intact bone. Therefore in this study the flight time was recorded by calculating the time interval between the initiation of the input pulse to the first peak of the recorded acoustic signal. Other parameters such as maximum amplitude of acoustic signal which is the voltage value of the highest peak was also recorded. The final measurement was the amount of energy in the packet, which was calculated as the area under curve. To further calculate the changes in signal due to varying fracture or cut depth, phase shift was calculated between each signal using the signal from intact bone as reference. When white noise was used to drive the transducers, a Fast Fourier Transform was carried out on the captured output signal to calculate frequency spectrum and the peak frequency of the signal.

CHAPTER 3

PRELIMINARY STUDIES

3.1 Drive Signal Configuration

The signal used to drive the transducers is one of the important aspects of this study. Without the low transient pulse technology, conducting this study would be difficult. The first step of this study involved performing an experiment which compares the use of low transient pulse as the drive signal to the use of regular rectangular pulse.

At first the transmitter and receiver were arranged in a direct coupling position, which simulates an ideal situation where signals are being captured by receiver directly from the transmitter face plate without any material in between which would change the output captured. It was confirmed that the face plates of the transmitter and receiver were arranged exactly parallel to each other with small amount of ultrasound gel in between to provide a good medium for energy transfer. The range between which the pulse width of LTP was tuned was from 6.56 μs (410 counts) to 7.2 μs (450 counts). The best clean LTP shown in Figure 3.1 was obtained at pulse width of 7.04 μs (440 counts). The transmitter was connected directly to FPGA and the receiver was connected directly to the oscilloscope. The amplifier was not connected to the receiver in this experiment.

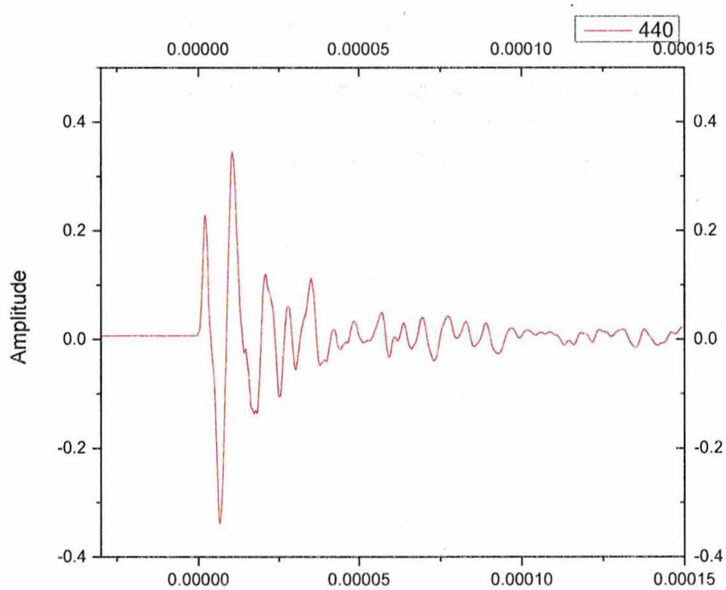

Figure 3.1 Low Transient Pulse generated with pulse period of 7.04 μs using the new FPGA system.

The second step involved confirming the efficiency of the use of LTP as a drive signal over the use of regular rectangular pulse. A simple experiment was carried out on the sheep tibia using the two transducers, one being the transmitter and other being the receiver. The distance between the transmitter and receiver was 35 mm. First a regular rectangular pulse wave with pulse period of 2500 μs, generated by signal generator was used to drive the acoustic transducer and an acoustic output signal captured by the receiver was recorded using the oscilloscope. The FPGA was then set up to generate Type 0 LTP (one pulse LTP) with pulse period of 7.16 μs which was then used to drive the transmitter. The output was again captured using oscilloscope. The FPGA setup was then changed to generate a Type 1 LTP (two pulse LTP). Figure 3.2 below shows the three acoustic output signals captured. From the Figures it can be confirmed that the LTP drive signal produced a much shorter, cleaner signal with less reflection waveforms, compared to the output captured using regular rectangular pulse drive signal. Type 1 LTP is also successful in reducing peaks observed in the secondary reflection signals in the output.

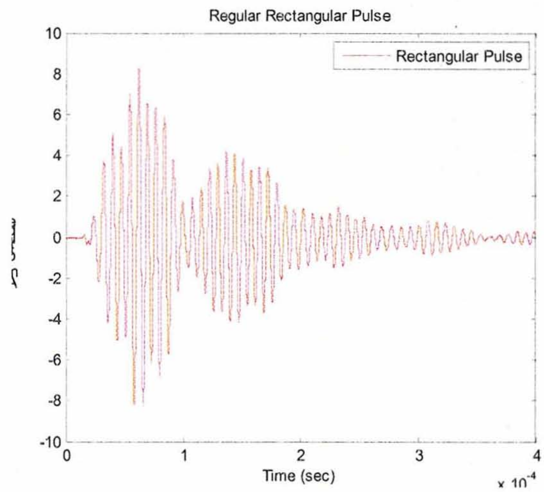

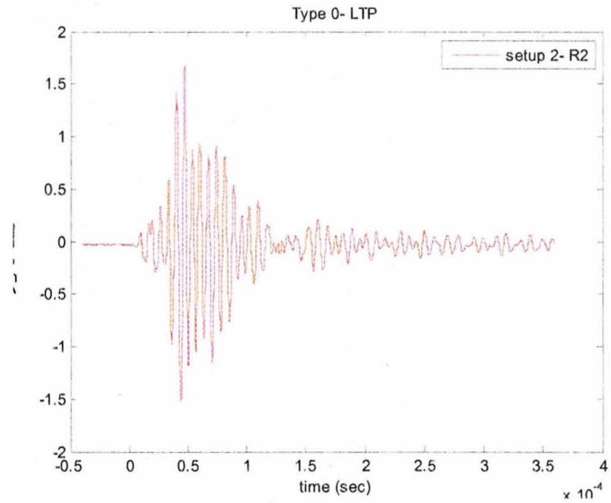

Figure 3.2a Output captures using regular rectangular pulse as the drive signal.

Figure 3.2b Output captured using Type 0 LTP (one pulse method) as the drive signal.

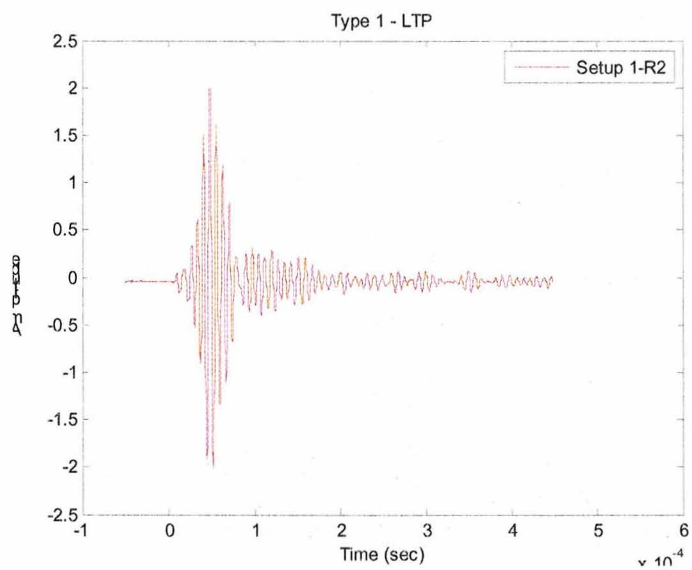

Figure 3.2c Output captured using Type 1 LTP (Two pulse method) as the drive signal.

To further determine the efficiency of using LTP as drive signal over the regular rectangular pulse, the coefficient of variance was calculated for the flight time and the maximum amplitude of the acoustic signal captured at different fracture depth. From results shown in Figure 3.3 it can be inferred that the frequency and the magnitude of error involved in using rectangular pulse is much higher compared to LTP. The results in Figure 3.3 indicate that LTP produces more consistent results at different fracture depth.

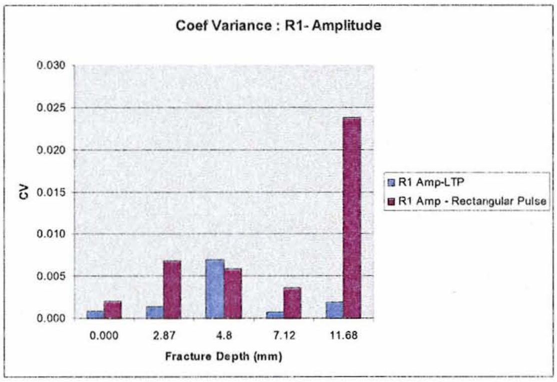

Figure 3.3a Coefficient of Variance of LTP and RMP in the amplitude at R1.

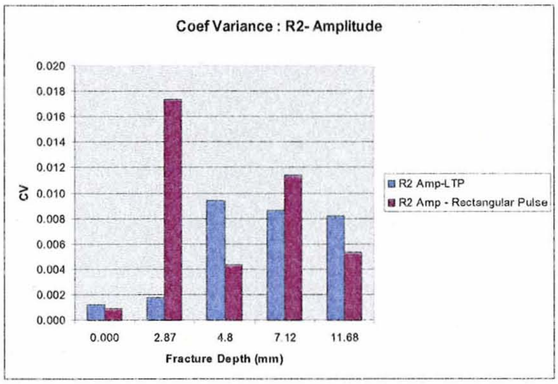

Figure 3.3b Coefficient of Variance of LTP and RMP in amplitude at R2.

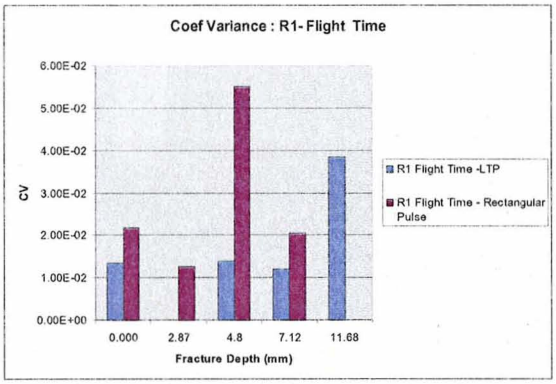

Figure 3.3c Coefficient of Variance of LTP and RMP in the flight time at R1.

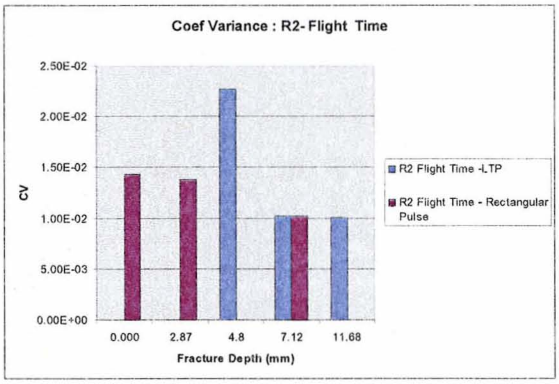

Figure 3.3d Coefficient of Variance of LTP and RMP in amplitude at R2.

3.2 Transducer Characteristics

The transducer characteristics were examined before the actual experiments for this study were performed. The variability between each transducer was the key characteristic that needed to be established. Although all four transducers were the same model and had the same specifications, purchased from the one manufacturer, some chance of variability may exist between each transducer. The possibility of variability required ensuring that the output captured at a specific position does not change for different receiver. In order to prove the absence of variability, an experiment was carried out where the position of transducer # 1 which was receiver 1 and transducer # 3 which was receiver 2 were switched. Plots shown in Figure 3.4 compare output captured by transducer # 1 and # 2 at each position as receiver 1 and receiver 2.

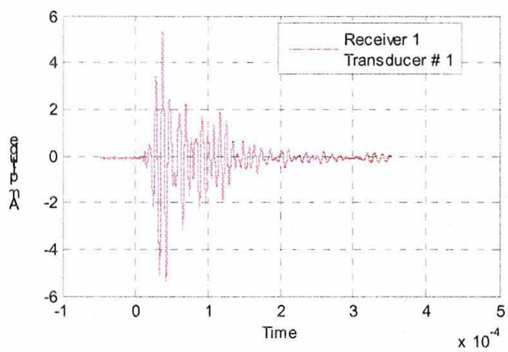

Figure 3.4a Transducer #1 at position 1.

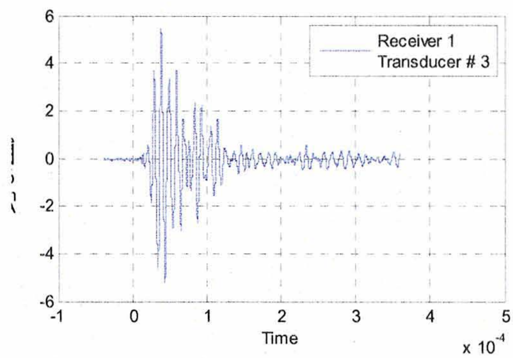

Figure 3.4b Transducer #3 at position 1.

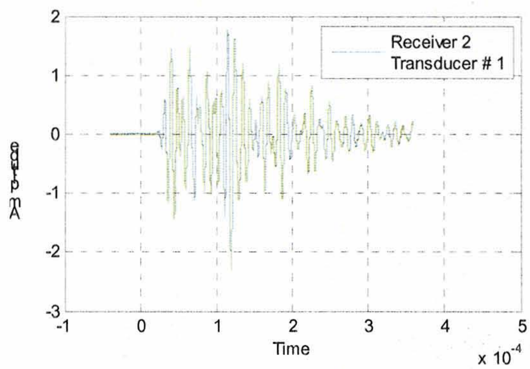

Figure 3.4c Transducer #1 at position 2.

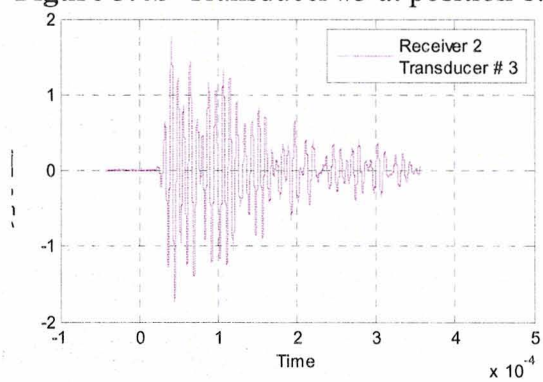

Figure 3.4d Transducer #3 at position 2.

The plots shown above clearly indicate that even though the order of the transducer is changed the output captured by a transducer still matches with output captured with a different transducer at the same position. This guarantees that the characteristics and functionality of each transducer is exactly the same and the change in their order does not affect the consistency of the results of the experiment.

The presence of linearity in data collection had to be established. A set of experiments were carried out to ensure that the acoustic energy captured by the receivers originates from the transmitter only and no other possible source. The first experiment involved three transducers on the sawbone plate, two of the three transducers were used as a transmitter and the third one was the receiver shown in Figure 3.5. As shown in Figure 3.5b and 3.5c the next two experiments involved just using one transmitter and one receiver at a time without changing the distance between each other.

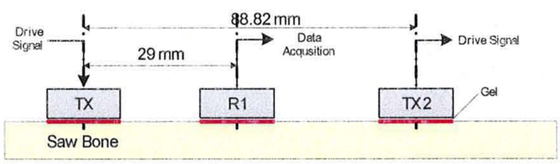

(a)

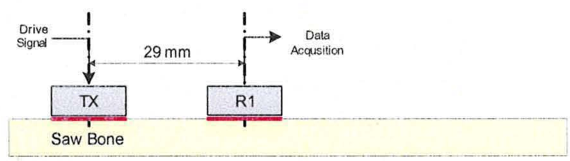

(b)

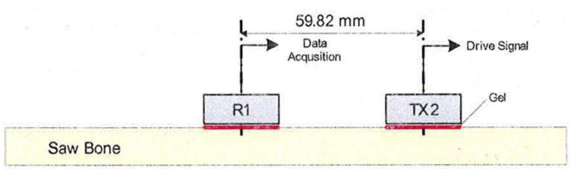

(c)

Figure 3.5a Experimental setup showing two active transmitters and one receiver.

Figure 3.5b Experimental setup showing one active transmitters and one receiver.

Figure 3.5c Experimental setup showing one active transmitters and one receiver.

The signals captured by the receiver from having only one active transmitter were added together and compared to the output signal captured by receiver having two active transmitters. This was done to compare if the sum of two separate signals from each transmitter matches the output signal captured when both transmitters were running simultaneously. The results from this experiment are shown in Figure 3.6. From the results it is clearly evident that sum of signals matches with the experimental data captured when two transmitters were generating drive signal simultaneously. This indicates the presence of linearity in the collection of data.

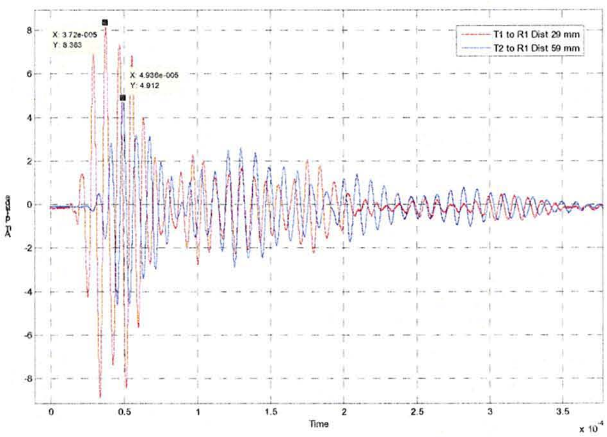

Figure 3.6a Output captured (Red) using only Transmitter 1 and output captured (Blue) using only Transmitter 2.

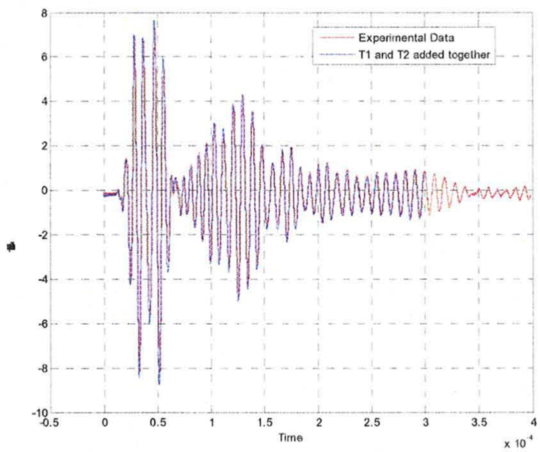

Figure 3.6b Experimental data (Red) captured when both transducers were running compared to sum of the two outputs (Blue) captured when transducer were used individually.

3.3 Mapping of Echoes

Before initiating the main experiments in this study it was of primary interest to understand the variables and factors involved in originating echoes in recorded acoustic signal by the receivers. Several series of experiments and mathematical analysis were performed to distinguish the unwanted echoes from the leading edge in the recorded acoustic signal. A better understanding of the signal contents allows quantification of the data with lower error margin and allows only the unwanted data to be discarded.

3.3.1 Simulation Analysis

A program was designed in SIMULINK to simulate and recreate the waveform which matches the experimental data which was recorded by the receiver. Figure 3.7 shows the block diagram of the program constructed in simulink to generate waveforms. This program uses a clean leading edge from the acoustic signal captured by receiver on the sawbone plate as a reference waveform. The program then uses the same leading edge

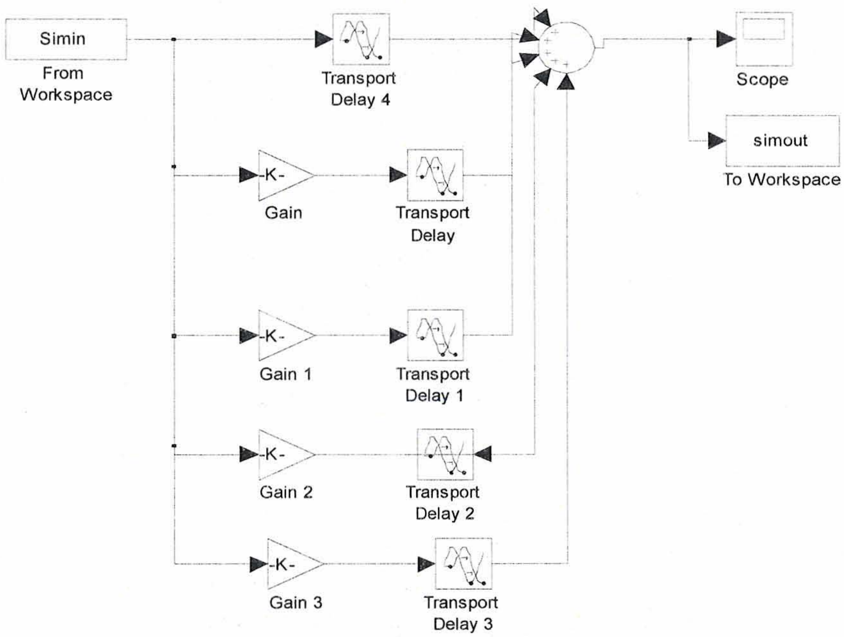

Figure 3.7 Block diagram of program constructed in simulink to generate waveform which matches experimental data.

and manipulates it by changing its flight time and amplitude and then combines it to the original leading edge. By doing this, a waveform can be generated to match the experimental data. Figure 3.8 shows a plot where the experimental waveform is compared to the waveform generated in simulink by manipulating four leading edges. From Figure 3.8 it can be inferred that the two waveforms fairly match each other. This indicates that most of the reflections captured are leading edges themselves with different amplitude and flight time.

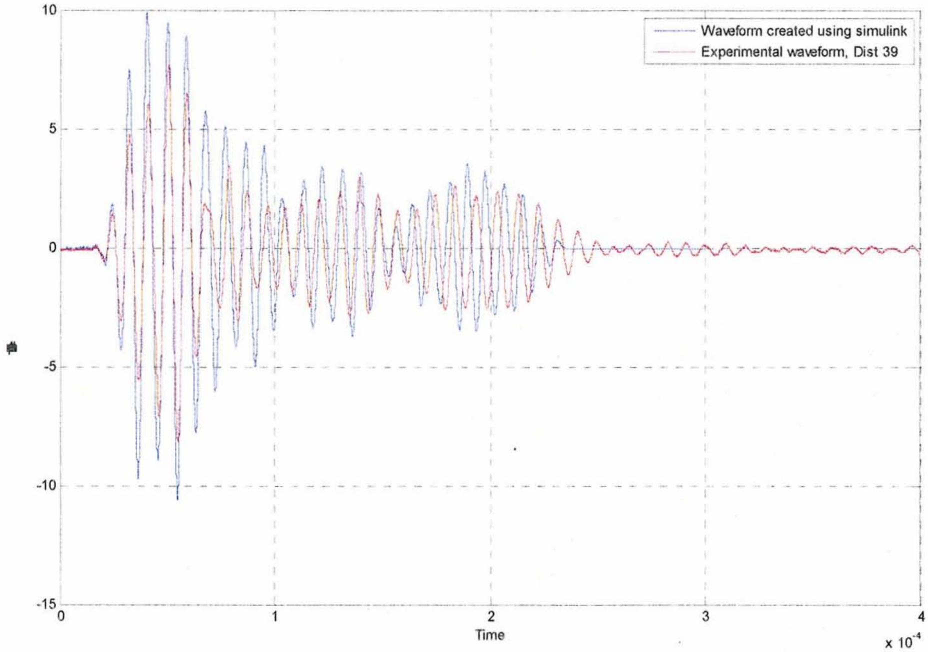

Figure 3.8 Comparing experimental (red) waveform to waveform generated in simulink (blue).

3.3.2 Mapping Origin of Echoes

Mapping the origins of the echoes present in the acoustic signal was one of the important milestones for this study. At first it was necessary to check if the four edges of sawbone plate are responsible for generating any reflections which are captured by the receiver. The technique used was to extend the boundary of the sawbone in all four directions by adding additional sawbone plates with ultrasound gel in between the plates. If the edges of sawbone plate are responsible for the generation of echoes then extension of the edge should allow acoustic energy to travel further before they are reflected by the boundary or totally depleted due to attenuation factor of the sawbone plate. Figure 3.9 compares the outputs captured by receiver in different arrangements, with each arrangement extending the boundary of sawbone plate in each direction.

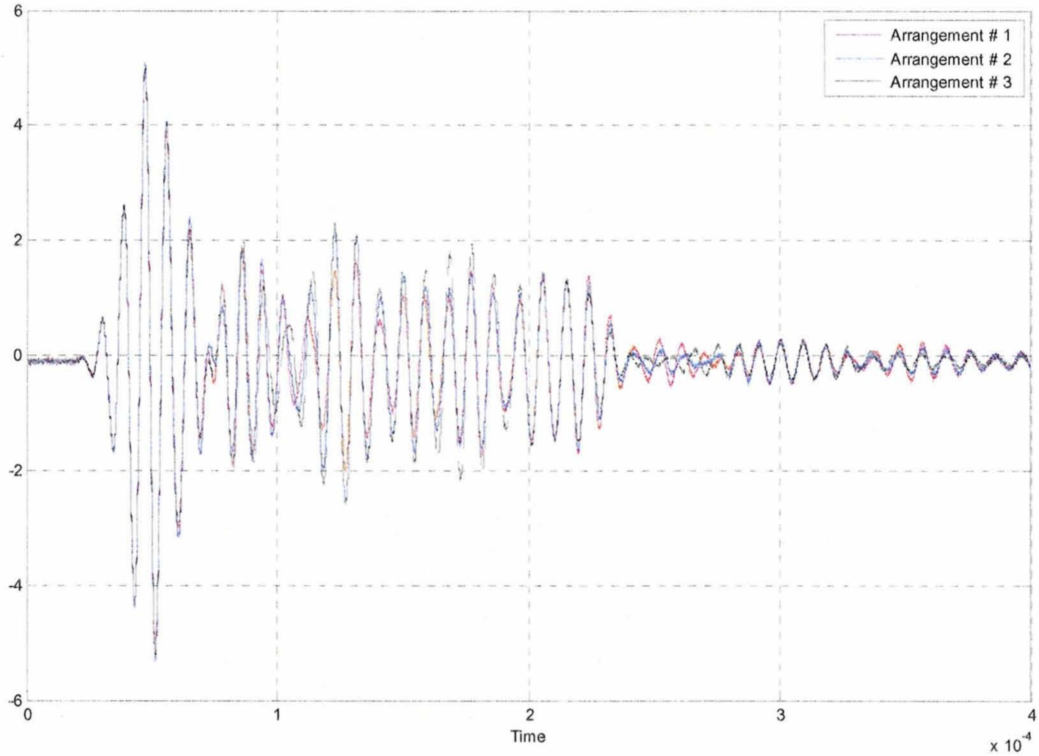

Figure 3.9 Compares the outputs captured in different arrangement which extend the boundary of the sawbone plate each time.

From the plots shown in Figure 3.9 it can be seen that acoustic signal captured in all three arrangements match each other. This indicates that the extension of the boundary failed to delay the arrival of reflected signal, therefore confirming that the presence of the edges perpendicular to the axial placement of the transducers do not result in strong echoes which can be captured by the receiver. Results also convey that the echoes are probably originated from the bottom surface of the sawbone plate which is parallel to transducer placement.

An experiment was carried out in order to further confirm that the most of the echoes originated from the inner boundary of the cortical bone or the bottom surface of the sawbone plate. In this experiment two sawbone plates were stacked on top of each other. The distance between transmitter and receiver was 29 mm. For the first case of experiments, data was captured without having any ultrasonic gel between the two stacked plates. For the second case of this experiment, a layer of ultrasound gel was applied between the two stacked plates. The output signal captured from each setup is shown below in Figure 3.10. Figure 3.10a shows presence of only two distinct waveforms.

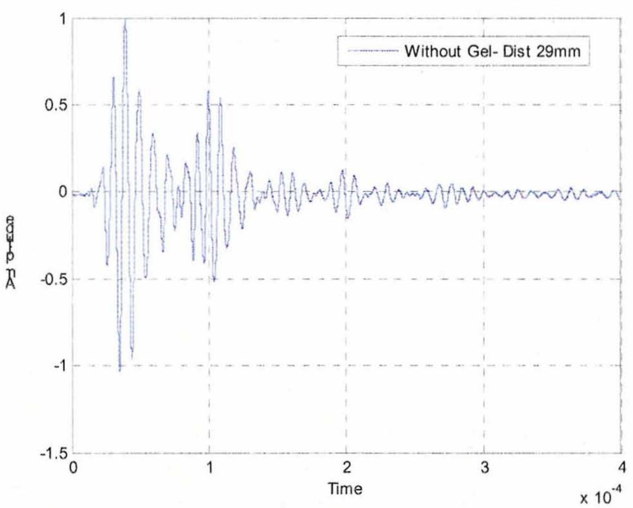

Figure 3.10a Output signal captured on two sawbone plates stacked on top of each other without ultrasound gel in between.

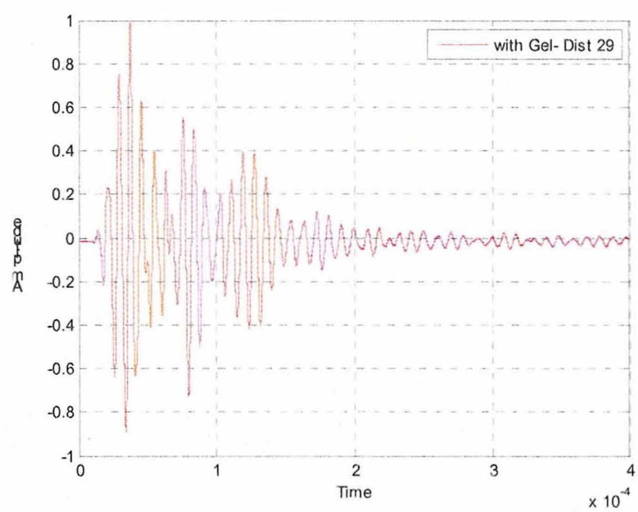

Figure 3.10b Output signal captured on two sawbone plates stacked on top of each other with layer of ultrasound gel between the two plates.

In the case where no ultrasound gel was used between the two plates it is trivial to consider the first leading edge to be the surface wave since it has the shortest path to the receiver and the second waveform originated from reflecting the bottom surface of the top sawbone plate. Figure 3.10b shows presence of three distinct waveforms. The presence of ultrasound gel between the two sawbone plates allows easy transfer of acoustic energy which produces an additional (third) waveform which was originated from reflection from the surface of the second sawbone plate. These results confirm the statement that most of the echoes in the captured acoustic signal originate from the lower surface of the specimen which is parallel to the surface where transducers are placed.

CHAPTER 4

RESULTS AND ANALYSIS

4.1 Fracture Detection by Regular Rectangular Pulse and LTP

An experiment was performed on a fractured sawbone plate to examine the ability of fracture detection of the LTP method and regular rectangular pulse. A 400 Hz rectangular pulse train with pulse width of 25 μs was applied to the transducer and output was captured. This captured output was then compared to the output captured by using a type-0 LTP which is a 400 Hz pulse train with pulse width of 7.16 μs (approximate 1 oscillation period). The setup 1 configuration used for this experiment is shown in Figure 4.1

Figure 4.1 Experimental setup for comparison of the LTP method and regular rectangular drive signal on the fracture detection.

Experimental data were captured through receiver 1 (R1) and receiver 2 (R2), located before and after the crack, respectively. Plotted in Figure 4.2a and 4.2b are received signals at R1 for the LTP and rectangular pulse, respectively. While the received signal at R2 for rectangular drive is plotted in Figure 4.3a, the response to LTP drive is shown in Figure 4.3b. As shown in Figures 4.2c and 4.3c, the LTP drive method produces a shorter duration and lower transient received signal compared to the rectangular one. Output signal captured at R2 using regular rectangular pulse (Figure 4.3a) represents a good example where high transient of rectangular pulse generates multiple peaks, which is likely to induce errors in identifying the leading edge and other signal parameters. At same time output signal captured at R2 using LTP pulse (Figure 4.3 b) represents only one peak which makes analyzing the signal parameters easier and accurate. The LTP method also shows better indication of the presence of the crack. This can be seen from the experimental results where the amplitude peak time shifted is clearer for the LTP method (Figures 4.2b and 4.3b) than that of the rectangular pulse (Figures 4.2a and 4.3a).

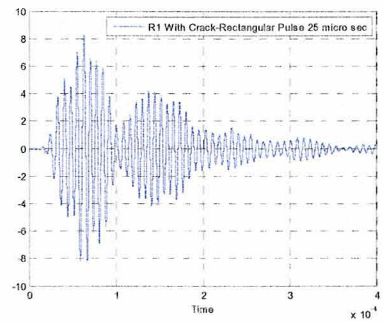

Figure 4.2a Signal received at R1 using regular rectangular pulse drive.

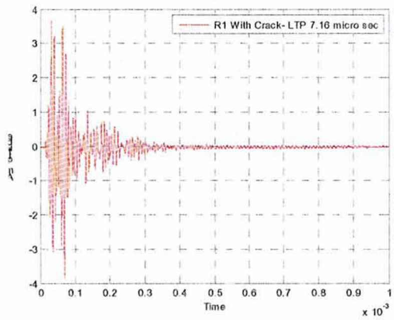

Figure 4.2b Signal received at R1 using LTP drive.

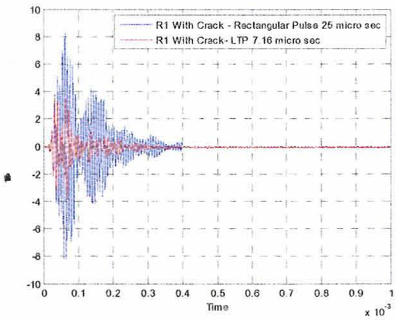

Figure 4.2c Comparison of the received signals at R1.

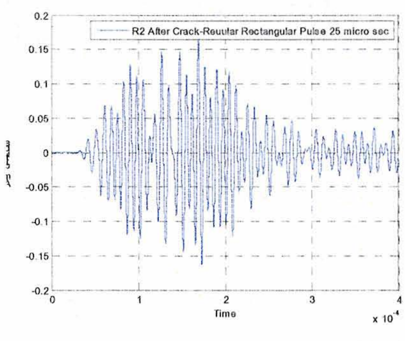

Figure 4.3a Signal received at R2 using regular rectangular pulse drive.

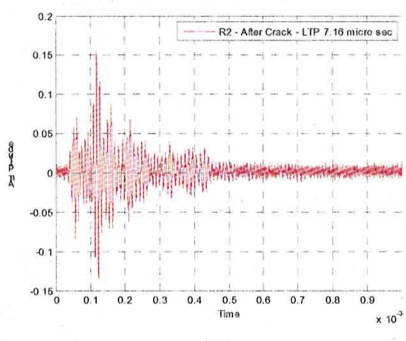

Figure 4.3b Signal received at R2 using LTP drive.

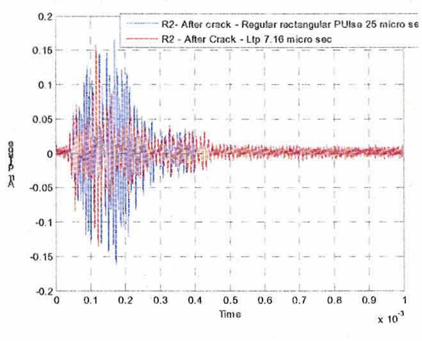

Figure 4.3c Comparison of the received signals at R2.

4.2 Sheep Tibia

Starting from intact bone, fractures were simulated in sheep tibia with depths of 2.87 mm, 4.80 mm, 7.12 mm and 11.68 mm. At each depth acoustic signals captured by R1 and R2 in both setup 1 and setup 2 were recorded using a digital oscilloscope. The distance between transducers and their setup for this experiment is shown in Figure 4.4. Type 0 LTP with the pulse period of 7.68 μs was used as a drive signal for this experiment. Three trials were carried out for each cut depth which involved detaching the glued bone and reattaching it with the same control amount of glue, and this process was repeated three times.

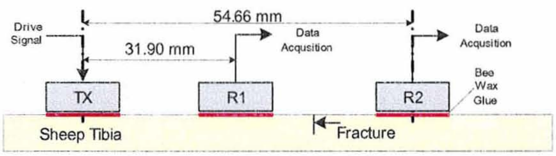

Figure 4.4a Setup 1 configuration.

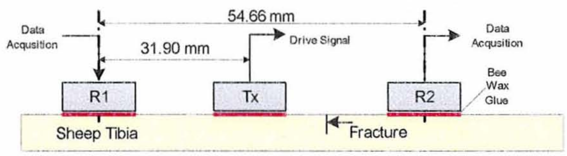

Figure 4.4b Setup 2 configuration.

All of the recorded signals from R1 and R2 for both setups were then analyzed and key parameters were calculated. The average values of flight time at R1 and R2 in both setups for each fracture depth are shown in Table 4.1 below. Figure 4.5 below gives a graphical representation of the behavior of flight time of the acoustic signal with respect to fracture depth.

Table 4.1 Average values of flight time of the signal at R1 and R2 for both setups

	Setup 1				Setup 2			
Depth (mm)	**R1 (sec)**	**R1 (σ) (sec)**	**R2 (sec)**	**R2 (σ) (sec)**	**R1 (sec)**	**R1 (σ) (sec)**	**R2 (sec)**	**R2 (σ) (sec)**
0	1.100e-5	±2.074e-21	1.813e-5	±2.309e-7	1.120e-5	±2.000e-7	9.800e-6	±0
2.87	1.113e-5	±1.154e-7	1.860e-5	±0	1.120e-5	±0	1.013e-5	±1.154e-7
4.80	1.107e-5	±1.154e-7	1.987e-5	±1.154e-7	1.127e-5	±1.154e-7	1.273e-5	±1.154e-7
7.12	1.100e-5	±2.074e-21	2.027e-5	±1.154e-7	1.120e-5	±2.000e-7	1.293e-5	±1.154e-7
11.68	1.127e-5	±1.154e-7	2.520e-5	±3.464e-7	1.120e-5	±0	1.507e-5	±4.618e-7

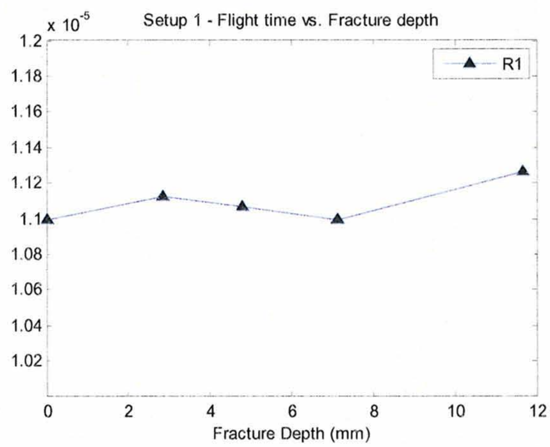

Figure 4.5a Flight time of acoustic signal captured by R1 in setup 1 vs. fracture depth.

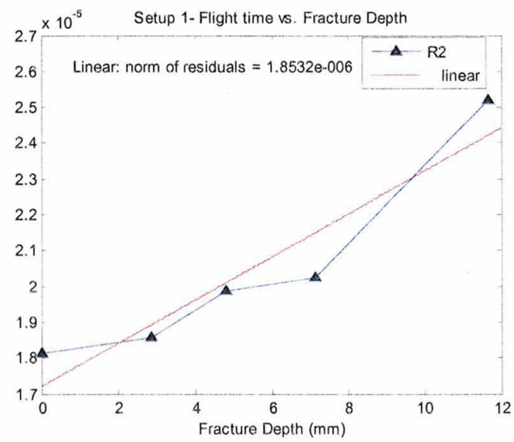

Figure 4.5b Flight time of acoustic signal captured by R2 in setup 1 vs. fracture depth.

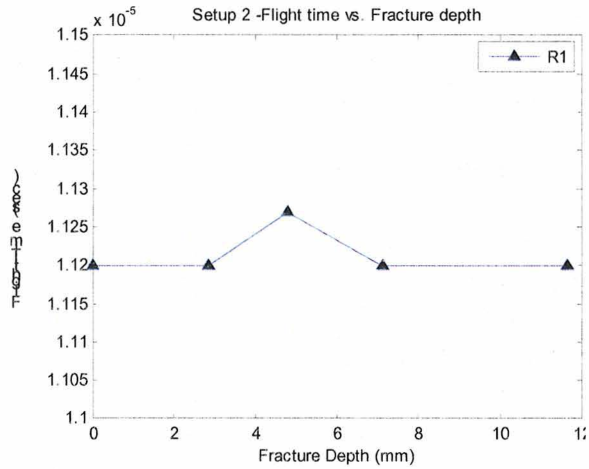

Figure 4.5c Flight time of acoustic signal captured by R1 in setup 2 vs. fracture depth.

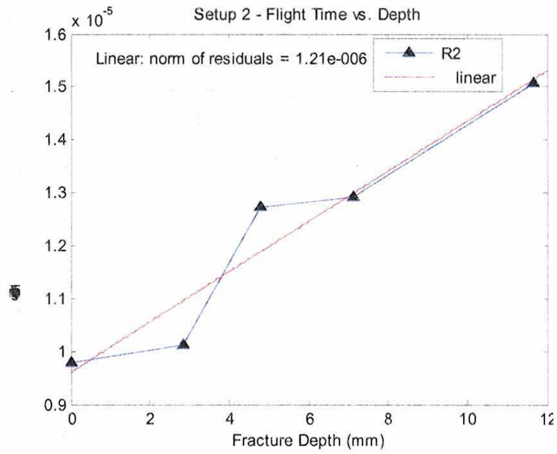

Figure 4.5d Flight time of acoustic signal captures by R2 in setup 2 vs. fracture depth.

From Figures 4.5b and 4.5d it can be inferred that the flight time of the acoustic signal for R2, which is the receiver mounted after the fracture for both setups undergoes an increase in its value with respect to the fracture depth. As expected the flight time values for R1 in both setups did not change significantly with change in fracture depth, confirming no effect of fracture on that section of the bone. The increase in flight time of acoustic signal with respect to the fracture depth indicates that the path of the acoustic waveform is being obstructed with presence of a discontinuity in material density of the bone. In an intact bone the acoustic wave travels longitudinally from receiver to transmitter, as it is considered to be the shortest wavepath. When a shallow cut is made to the bone the shortest wavepath is the one which goes under the cut and to the receiver. This wavepath is slightly longer (depending on the depth of cut) than one assumed in reality (which is the distance between transmitter and receiver), resulting in longer flight time. So deeper fractures results in longer pathways of acoustic signal and therefore longer flight time values.

The Table 4.2 below contains the averaged maximum amplitude values of recorded acoustic signal in both setups. Figure 4.6 shows the graphical representation of changes occurring to the peak amplitude values of the recorded signal with respect to the fracture depth. The maximum amplitude for the acoustic signal captured by R2 in both setup undergoes a linear drop as the fracture depth increases. Linear curve fitting for the amplitude vs. fracture depth plot yields a low residual value (0.0178 for setup 1 and 0.3943 for setup2). This low residual value for linear curve fitting and higher slope confirms the high sensitivity of maximum amplitude to a fracture in bone. The drop in maximum amplitude for receivers placed after the fracture indicates the increase in attenuation coefficient of the bone. Increase in fracture depth increases the area of discontinuity in bone which obstructs the clean transfer of acoustic energy through the medium and so maximum amplitude of the acoustic signal experiences a drop. Maximum amplitude of acoustic signal captured at R1 shows some fluctuations; however taking scale under consideration, these fluctuations in amplitude values are very small.

Table 4.2 Average values of maximum amplitude of the signal at R1 and R2 for both setups.

	Setup 1				**Setup 2**			
Depth (mm)	**R1**	**R1 (σ)**	**R2**	**R2 (σ)**	**R1**	**R1 (σ)**	**R2**	**R2 (σ)**
0	0.8282	± 0.0020	0.5137	±0.0002	0.8441	±0.0046	1.680	±0.0005
2.87	0.7705	± 0.0029	0.4329	±0.0004	0.8040	±0.0049	1.520	±0.1149
4.80	0.7464	± 0.0005	0.3880	±0.0002	0.8141	± 0.0030	1.626	±0.0012
7.12	0.8236	± 0.0020	0.3547	±0.0006	0.8177	±0.0025	1.303	±0.0092
11.68	0.7532	±0.0005	0.2471	±0.0010	0.7692	±0.0005	0.675	±0.0025

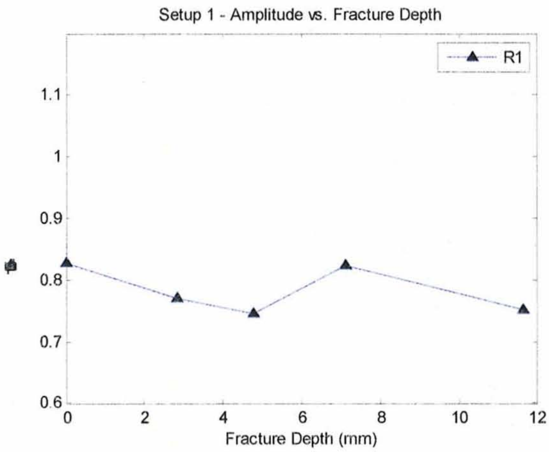

Figure 4.6a Maximum amplitude of acoustic signal captures by R1 in setup 1 vs. fracture depth.

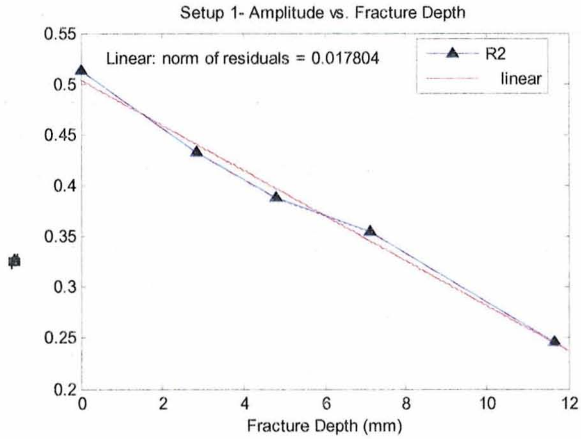

Figure 4.6b Maximum amplitude of acoustic signal captures by R2 in setup 1 vs. fracture depth.

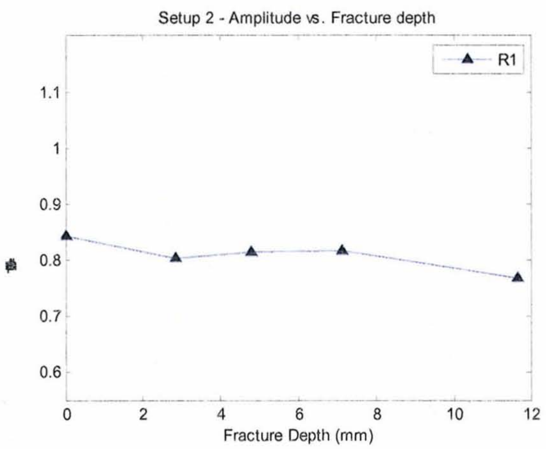

Figure 4.6c Maximum amplitude of acoustic signal captures by R1 in setup 2 vs. fracture depth.

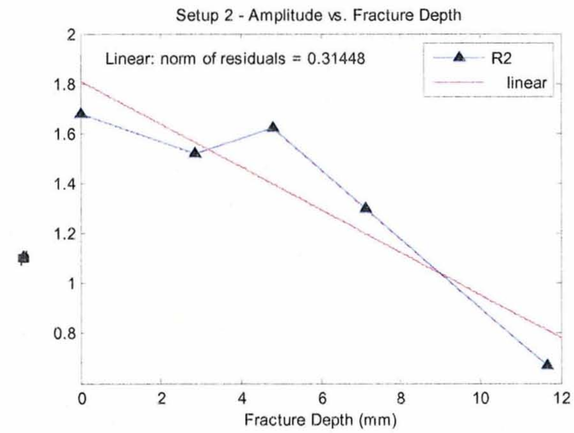

Figure 4.6d Maximum amplitude of acoustic signal captures by R2 in setup 2 vs. fracture depth.

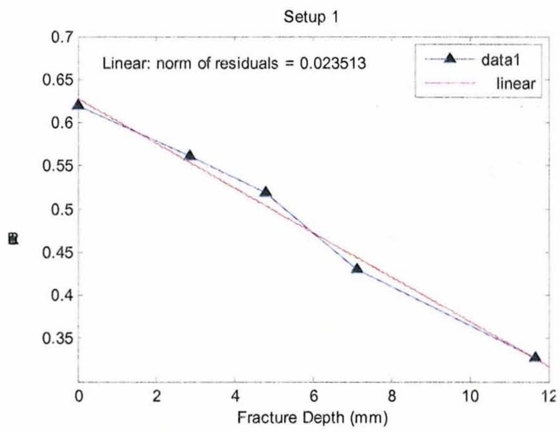

Figure 4.6e Ratiometric (R2/R1) representation of maximum amplitude of setup 1 vs. fracture depth.

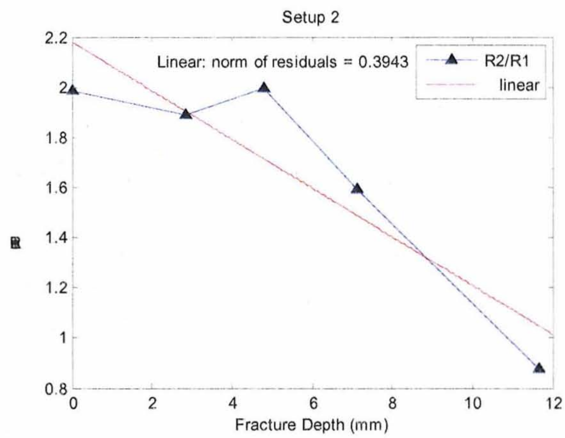

Figure 4.6f Ratiometric (R2/R1) representation of maximum amplitude of setup 2 vs. fracture depth.

To get a better illustration of changes in the entire signal shape due to fracture, phase shifts between each output captured by R2 for both setups for all cut depth were calculated. The signal recorded on intact bone was used as the reference to calculate the phase shift. Tables 4.3 and 4.4 contains the values of phase shift in degrees. Table 4.3 shows a steady increase in phase angle for output captured in setup 1 but output captured in setup 2 fails to follow the same trend. The short distance between transmitter and R2 in setup 2 can be responsible for this disturbance in linear trend of phase angle seen in setup 1. Since the distance is short between the two transducers the reflection waves are more likely to be detected along with leading edge. This multi-pass situation might be responsible for creating interference in data and creating the disturbance in trend. From Tables 4.3 and 4.4 it can also be inferred that phase angle measurement loses its sensitivity as the fracture depth increases. The steady increase in phase angle in setup1 with respect to the fracture depth confirms that the path taken by the waveform becomes longer as cut progresses.

Table 4.3 Phase shift values for acoustic signal captured by R2 in setup 1.

Depth (mm)	Highest Peak Time	Phase Angle
0	5.56E-05	0
2.87	5.60E-05	23.2
4.80	5.62E-05	34.8
7.12	5.64E-05	46.5
11.68	5.64E-05	46.5

Table 4.4 Phase shift values for acoustic signal captured by R2 in setup 2.

Depth (mm)	Highest Peak Time	Phase Angle
0	4.76E-05	0
2.87	4.80E-05	21.2
4.80	4.78E-05	10.6
7.12	4.82E-05	31.8
11.68	4.82E-05	31.8

Correlation analysis was carried out on all the acoustic waveform captured during this study. The acoustic signal from R1 and R2 captured on the intact bone was used as the reference signal. All the other signals were correlated to the respective reference signals. Correlation coefficient was computed which provides an index variable that indicates how different the acoustic signal captured at different cut depth is to the reference signal.

Table 4.5a Correlation coefficient values of acoustic signal captured in setup1.

Fracture Depth (mm)	Correlation coef. R1	Correlation coef. R2
0	1	1
2.87	0.9565	0.7987
4.80	0.9217	0.6996
7.12	0.8746	0.5169
11.68	0.9094	0.4364

Table 4.5b Correlation coefficient values of acoustic signal captured in setup 2.

Fracture Depth (mm)	Correlation coef. R1	Correlation coef. R2
0	1	1
2.87	0.9576	0.9145
4.80	0.9397	0.9023
7.12	0.8958	0.7923
11.68	0.902	0.7944

From Figures 4.5b and 4.5d it can be seen that the flight time value in both setups for shallow fracture only increased by a small interval indicating low sensitivity. This small increase in flight time for fracture depth of 2.87 mm indicates that proper detection of small fractures just by using flight time of acoustic signal is difficult. At the same time, maximum amplitude vs. fracture plots (Figure 4.2 b and d) show steady and high sensitivity for all fracture depths. Careful selection of each signal parameter by an algorithm will allow quantifying the fracture characteristics accurately. When the fracture depth is small, the flight time of the acoustic output can be used in conjunction with the maximum amplitude and the phase shift of the acoustic output which would support the low sensitivity of flight time in shallow cuts. Similarly, if the fracture is deep, the flight time of acoustic output along with its maximum amplitude will be the ideal parameters. This would eliminate the low sensitivity of phase angle in deeper fractures.

the sawbone plate using the bee wax. At each depth, the acoustic signal captured by R1 and R2 in setup 1 were recorded using a digital oscilloscope. The distance between transducers and their setup for this experiment is shown in Figure 4.7 below. Frequency spectrum analysis was carried out on the on the output signal captured by R1 and R2. Table 4.6 shows the peak frequency recorded at each cut depth. Figure 4.8 shows that before the crack was introduced the value of peak frequency for R1 and R2 is identical which indicated a presence of a common dominant resonant frequency of the sawbone plate. As cracks were introduced the peak frequency at R1 and R2 experienced a drop in peak frequency.

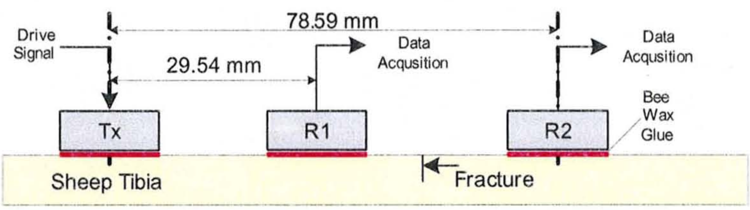

Figure 4.7 Setup configuration.

R2 which is the transducer mounted after crack observed a drop of higher value compared to R1 once the crack was introduced to the plate. A successive drop in peak frequency was observed as the crack depth increased. This gradual drop in frequency shows that when shallow cuts are introduced in sawbone plate, the plate losses its ability to resonate as one intact specimen. When cut of depths 2.68 mm and 2.83 mm were made to the sawbone plate which were beyond the half thickness of the plate, the peak frequency for R1 and R2 spiked up to their initial peak frequency. This sudden increase in peak frequency with cuts with higher depth indicates that the sawbone plate retains its original dominant frequency of 129 KHz. Same concept can be applied to detect fractures in bone. Recording two different peak frequencies along bone would indicate the presence of a defect.

Table 4.6 Peak frequency captured at R1 and R2 for each cut depth.

Cut Depth (mm)	R1 (KHz)	R2 (KHz)
0	129	129
1.5	125	121
2.3	115	109
2.68	125	127
2.83	130	127

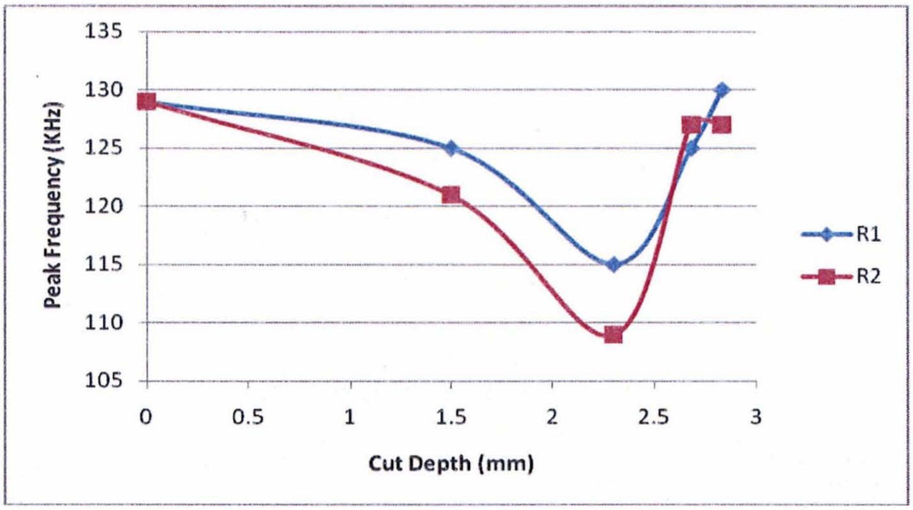

Figure 4.8 Plot showing the behavior of the peak frequency of acoustic signal recorded at R1 and R2 with respect to different cut depths.

CHAPTER 5

CONCLUSION

The method of using low transient pulse as drive signal has been proposed as a new modality in bone fracture detection based on flight time, maximum amplitude and peak frequency of the acoustic signal. The use of a low transient pulse greatly increased the resolution and reduced reflections in acoustic signal when compared to regular rectangular pulse. This increase in resolution supports the application of axial quantitative ultrasound technique to detect bone defects. The three transducer placement method used in this study provided a reference reading which is unaffected by the fracture and a reading which is affected by the fracture. This reference reading allows the injured bone to act as its own calibration standard.

Through a series of tests which involved simulating fractures of different depths in sheep tibia, behavioral patterns of different signal parameters with respect to depth of a fracture was established. Flight time, maximum amplitude, phase angle and peak frequency when used in different combinations determines the depth of the fracture. This proves that an acoustic signal can be quantified to yield the condition of a fracture in bone.

Using the behavioral patterns of the signal parameters established in this study, an algorithm can be generated which would determine the fracture condition by comparing signal parameters from R1 to signal parameters of R2. Through this study it is shown that the low transient pulse technology opens up the possibility of using ultrasound to detect small defects in bone which are missed by normal conventional fracture detection methods. An ultrasound device to detect bone defects will quantify the results, eliminating the need of an skilled technician to interpret the results.

APPENDIX A

SHEEP TIBIA RAW DATA

Fracture Depth 0 mm

Setup 1: **Tx --> R1 --> Fx -->R2**

Receiver		Peak Amplitude	Area	Flight time	Peak Frequency (KHz)
R1	Trial # 1	0.8271	225.87	1.10E-05	136.7
	Trial # 2	0.8252	236.96	1.10E-05	136.7
	Trial # 3	0.8232	222.73	1.10E-05	136.7
R2	Trial # 1	0.5117	133.27	1.80E-05	117.2
	Trial # 2	0.5137	183.56	1.84E-05	117.2
	Trial # 3	0.5156	166.6	1.80E-05	117.2

Setup 2: R1 --> Tx --> Fx -->R2

Receiver		Peak Amplitude	Area	Flight time	Peak Frequency (KHz)
R1	Trial # 1	0.8477	292.39	1.10E-05	139.2
	Trial # 2	0.8389	277.33	1.14E-05	139.2
	Trial # 3	0.8457	279.56	1.12E-05	139.2
R2	Trial # 1	1.681	437.19	9.80E-06	141.6
	Trial # 2	1.681	422.45	9.80E-06	141.6
	Trial # 3	1.68	435.24	9.80E-06	141.26

Fracture Depth of 2.87 mm

Setup 1: Tx --> R1 --> Fx -->R2

Receiver		Peak Amplitude	Area	Flight time	Peak Frequency (KHz)
R1	Trial # 1	0.7705	265.62	1.12E-05	122.1
	Trial # 2	0.7734	252.79	1.12E-05	122.1
	Trial # 3	0.7676	170.34	1.10E-05	122.1
R2	Trial # 1	0.4332	193.25	1.86E-05	163.6
	Trial # 2	0.4324	193	1.86E-05	163.6
	Trial # 3	0.4332	192.55	1.86E-05	163.6

Setup 2: R1 --> Tx --> Fx -->R2

Receiver		Peak Amplitude	Area	Flight time	Peak Frequency (KHz)
R1	Trial # 1	0.8047	215.07	1.12E-05	122.1
	Trial # 2	0.7988	280.37	1.12E-05	122.1
	Trial # 3	0.8086	271.48	1.12E-05	122.1
R2	Trial # 1	1.456	367.53	1.02E-05	141.6
	Trial # 2	1.452	417.05	1.02E-05	141.6
	Trial # 3	1.653	338.51	1.00E-05	141.6

Fracture Depth of 4.80 mm

Setup 1: **Tx --> R1 --> Fx -->R2**

Receiver		Peak Amplitude	Area	Flight time	Peak Frequency (KHz)
R1	Trial # 1	0.7461	260.18	1.12E-05	122.1
	Trial # 2	0.7471	269.78	1.10E-05	122.1
	Trial # 3	0.7461	251.49	1.10E-05	122.1
R2	Trial # 1	0.3781	162.79	2.00E-05	117.12
	Trial # 2	0.3777	160.49	1.98E-05	117.12
	Trial # 3	0.3781	158.92	1.98E-05	117.12

Setup 2: R1 --> Tx --> Fx -->R2

Receiver		Peak Amplitude	Area	Flight time	Peak Frequency (KHz)
R1	Trial # 1	0.8115	284.87	1.12E-05	122.1
	Trial # 2	0.8174	217.51	1.12E-05	122.1
	Trial # 3	0.8135	271.45	1.14E-05	122.1
R2	Trial # 1	1.625	408.13	1.28E-05	141.6
	Trial # 2	1.627	413.03	1.26E-05	141.6
	Trial # 3	1.625	401.04	1.28E-05	141.6

Fracture Depth of 7.12 mm

Setup 1: **Tx --> R1 --> Fx -->R2**

Receiver		Peak Amplitude	Area	Flight time	Peak Frequency (KHz)
R1	Trial # 1	0.8252	307.03	1.10E-05	122.1
	Trial # 2	0.8242	302.72	1.10E-05	122.1
	Trial # 3	0.8213	309.04	1.10E-05	122.2
R2	Trial # 1	0.3551	158.49	2.04E-05	117.2
	Trial # 2	0.3551	158.49	2.02E-05	117.2
	Trial # 3	0.3539	156.68	2.02E-05	117.2

Setup 2: R1 --> Tx --> Fx -->R2

Receiver		Peak Amplitude	Area	Flight time	Peak Frequency (KHz)
R1	Trial # 1	0.8203	307.17	1.14E-05	122.1
	Trial # 2	0.8174	309.98	1.12E-05	122.1
	Trial # 3	0.8154	316.18	1.10E-05	122.1
R2	Trial # 1	1.305	339.21	1.28E-05	141.6
	Trial # 2	1.293	353.03	1.30E-05	141.6
	Trial # 3	1.311	374.39	1.30E-05	141.6

Fracture Depth of 11.68 mm

Setup 1: **Tx --> R1 --> Fx -->R2**

Receiver		Peak Amplitude	Area	Flight time	Peak Frequency (KHz)
R1	Trial # 1	0.7529	289.26	1.12E-05	122.1
	Trial # 2	0.7539	291.82	1.12E-05	122.1
	Trial # 3	0.7529	312.78	1.14E-05	122.1
R2	Trial # 1	0.2467	102.78	2.48E-05	117.2
	Trial # 2	0.2463	57.008	2.54E-05	117.2
	Trial # 3	0.2482	99.426	2.54E-05	117.2

Setup 2: R1 --> Tx --> Fx -->R2

Receiver		Peak Amplitude	Area	Flight time	Peak Frequency (KHz)
R1	Trial # 1	0.7695	332.76	1.12E-05	122.1
	Trial # 2	0.7695	343.44	1.12E-05	122.1
	Trial # 3	0.7686	328.67	1.12E-05	122.1
R2	Trial # 1	0.6719	212.42	1.56E-05	141.6
	Trial # 2	0.6768	215.73	1.48E-05	141.6
	Trial # 3	0.6748	253.71	1.48E-05	141.6

REFERENCES

Beck, B. R. (1998). "Tibial stress injuries. An aetiological review for the purposes of guiding management." Sports Med **26**(4): 265-79.

Bennell, K. L. and P. D. Brukner (1997). "Epidemiology and site specificity of stress fractures." Clin Sports Med **16**(2): 179-96.

Brukner, P. (2000). "Exercise-related lower leg pain: bone." Med Sci Sports Exerc **32**(3 Suppl): S15-26.

Callahan, L. R., M. F. Dillingham, et al. (2001). Sports Med: athletic injuries.

Camus, E., M. Talmant, et al. (2000). "Analysis of the axial transmission technique for the assessment of skeletal status." J Acoust Soc Am **108**(6): 3058-65.

Chang, T. N., Hou, et al. (2003). "Optimal input shaper design for high speed robotic workcells." Journal of Vibration and Control **9**(12): 1359-1376.

Cheng, B. and T. Chang (2007). "Enhancing ultrasonic imaging with low transient pulse shaping." IEEE Trans Ultrason Ferroelectr Freq Control **54**(3): 627-35.

Coady, C. M. and L. J. Micheli (1997). "Stress fracture in the pediatric athlete " Clin Sports Med **16**: 225-38.

Fitzgerald, R. (2001). "Error in radiology." Clin Radiol **56**(12): 938-46.

Frost, M. L., G. M. Blake, et al. (2002). "A comparison of fracture discrimination using calcaneal quantitative ultrasound and dual X-ray absorptiometry in women with a history of fracture at sites other than the spine and hip." Calcif Tissue Int **71**(3): 207-11.

Hubner, U., W. Schlicht, et al. (2000). "Ultrasound in the diagnosis of fractures in children." J Bone Joint Surg Br **82**(8): 1170-3.

Knapp, K. M., G. M. Blake, et al. (2004). "Can the WHO definition of osteoporosis be applied to multi-site axial transmission quantitative ultrasound?" Osteoporos Int **15**(5): 367-74.

Lowet, G. and G. Van der Perre (1996). "Ultrasound velocity measurement in long bones: measurement method and simulation of ultrasound wave propagation." J Biomech **29**(10): 1255-62.

Maitra, R. S. and D. L. Johnson (1997). "Stress Fractures, Clinical history and physical examination." Clin Sports Med **16**: 259-74.

Missing Page

Monteleone, G. P. (1995). "Stress fracture in the athlete." Ortho Clin North Am **26**: 423-32.

Morris, J. M. (1968). "Fatigue fractures." Calif Med **108**(4): 268-74.

Sanderlin, B. W. and R. F. Raspa (2003). "Common stress fractures." Am Fam Physician **68**(8): 1527-32.

Sarvazyan, A., A. Tatarinov, et al. (2008). "Application of the dual-frequency ultrasonometer for osteoporosis detection." Ultrasonics.

Swischuk, L. E. and J. A. Hernandez (2004). "Frequently missed fractures in children (value of comparative views)." Emerg Radiol **11**(1): 22-8.

Tatarinov, A., N. Sarvazyan, et al. (2005). "Use of multiple acoustic wave modes for assessment of long bones: model study." Ultrasonics **43**(8): 672-80.